ASTRONOMY
AND
ASTROPHYSICS

Short-term spectroscopic variability in the pre-main sequence Herbig Ae star AB Aurigae during the MUSICOS 96 campaign[*]

C. Catala[1], J.F. Donati[1], T. Böhm[1], J. Landstreet[2], H.F. Henrichs[3], Y. Unruh[4], J. Hao[5], A. Collier Cameron[6],
C.M. Johns-Krull[7], L. Kaper[8], T. Simon[9], B.H. Foing[10], H. Cao[5], P. Ehrenfreund[11], A.P. Hatzes[12], L. Huang[5],
J.A. de Jong[3], E.J. Kennelly[13], E. ten Kulve[3], C.L. Mulliss[14], J.E. Neff[15], J.M. Oliveira[10], C. Schrijvers[3],
H.C. Stempels[11,10], J.H. Telting[16], N. Walton[16], and D. Yang[5]

[1] Laboratoire d'Astrophysique de l'OMP, CNRS UMR 5572, Observatoire Midi-Pyrénées, 14, avenue Edouard Belin,
F-31400 Toulouse, France
[2] Astronomy Department, University of Western Ontario, London, Ontario, Canada
[3] Astronomical Institute "Anton Pannekoek", University of Amsterdam, The Netherlands
[4] Institute for Astronomy, University of Vienna, Austria
[5] Chinese Academy of Sciences, Beijing Astronomical Observatory, P.R. China
[6] School of Physics and Astronomy, University of St-Andrews, Scotland
[7] JILA, University of Colorado, Boulder, CO, USA
[8] European Southern Observatory, Garching bei München, Germany
[9] Institute for Astronomy, University of Hawaii, USA
[10] Solar System Division, ESA Space Science Department, ESTEC, Noordwijk, The Netherlands
[11] Leiden Observatory, The Netherlands
[12] Astronomy Department, University of Texas, Austin, TX, USA
[13] High Altitude Observatory, Boulder, CO, USA
[14] Ritter Astrophysical Research Center, The University of Toledo, OH, USA
[15] Department of Astronomy, Penn State University, USA
[16] Isaak Newton Group, NFRA/ASTRON, Royal Greenwhich Observatory, La Palma, Spain

Abstract. We present results of the spectroscopic monitoring of AB Aur obtained during the MUSICOS 96 campaign. The analysis is mainly focussed on the He I D3 line, on the Hα line, and on a set of photospheric lines. The star was monitored irregularly for more than 200 hours.

We confirm the high level of variability of spectral lines in AB Aur. We find that the photospheric lines have a profile differing significantly from a classical rotational profile. The dominant features of this abnormal photospheric profile are a blue component, in absorption, whose velocity is modulated with a 34hr period, and a red component, stable in velocity but of variable intensity, with a possible periodicity near 43 hrs.

The He I D3 line exhibits two well-defined components: a blue component, always in emission with a velocity modulated with a 45hr period, and a red component of variable intensity, alternatively in emission and in absorption, occurring at a fixed velocity, with a variable intensity possibly modulated with a 45 hr period.

The Hα line, showing a P Cygni profile, also exhibits pseudo-periodic variations of its blue absorption component, but its variability appears more complicated than that of the other lines studied here.

We suggest that the blue component of the photospheric lines is modulated by the star's rotation, with a period of 34 hrs, due to a highly inhomogeneous photosphere, involving significant radial flows. Our model also involves downflows onto the stellar pole to account for the red components of the photospheric lines and of the He I D3 line.

We propose two different interpretations of the behavior of the blue component of the He I D3 line. In the first one, this component is formed in a wind originating from the star's equatorial regions. In this interpretation, the rotation period of the equatorial regions of the star is 45 hrs, implying a 25% surface differential rotation, with the pole rotating faster than the equator. The second interpretation involves a wind originating from a region of a circumstellar disk, at a distance of 1.6 stellar radii from the star's center, with a rotation period of 45 hrs. We are not able to decide which one of these two interpretations is more likely, on the basis of the data presented here.

1. Introduction

The Herbig Ae/Be stars are pre-main sequence objects with masses ranging from 2 to 5 $M_\odot$. A very significant fraction of them show conspicuous signs of strong stellar winds, such as P Cygni profiles at Hα and Mg II h & k, and of chromospheric activity, such as the presence of C IV and Si IV resonance lines, emission in Ca II K & the infrared triplet, and in the He I 5876 Å lines (Catala et al. 1986a).

AB Aurigae is the brightest Herbig Ae star of the northern hemisphere, and is often considered as the prototype of the whole class. A detailed analysis of its line profiles and continua led to a model of its outer layers, including a wind with a mass loss rate of 10^{-8} $M_\odot$ yr^{-1}, and an extended chromosphere with a maximum temperature of 17,000 K overlying a photosphere at 10,000 K (Catala & Kunasz 1987).

This wind is certainly not spherically symmetric. Indeed, the rotational modulation of lines formed in the wind (Mg II resonance lines, Ca II K) was interpreted as due to co-rotating streams, organized in an azimuthal structure controlled by a surface magnetic field, by analogy with the structure of the solar wind (Praderie et al. 1986; Catala et al. 1986b).

Besides, the changes of the Hα line profile from a type II P Cygni profile to a single emission was interpreted by Pogodin (1992) in terms of an equatorial wind model, in which the opening angle of the wind is variable and controlled by a magnetic field.

The picture which emerges from these previous analyses is that of a complex wind, with both a latitudinal and azimuthal structure, probably controlled by a magnetic field. However, this model is far from being well established and needs observational confirmation. Furthermore, no magnetic detection of AB Aur has been reported so far, in spite of several attempts.

The MUSICOS 96 campaign on AB Aur constituted a major effort to better understand the photosphere and wind of this star, and a further attempt at detecting directly a surface magnetic field. The main goal of the AB Aur observations during the MUSICOS 96 campaign was the monitoring of photospheric lines, and a selection of chromospheric and wind lines, such as the He I D3 lines, and the Hα line.

The present paper deals with the short-term variability of these lines. In Sect. 2, we review the conclusions of previous related work. The observations and data reduction procedures are presented in Sect. 3. The observed variability is described in Sect. 4, and discussed in Sect. 5 in terms of a photosphere-wind model involving localized outflows affecting the formation of photospheric lines and He I D3 lines. A general conclusion is given in Sect. 6.

2. Previous related work

Catala & Kunasz (1987) proposed a quantitative model of the wind of AB Aur. This model involves a spherically symmetric wind with a mass loss rate of about 10^{-8} $M_\odot$ yr^{-1}, with velocities reaching up to 300–400 km s^{-1}, and an extended chromosphere at the base of the wind, with temperatures as high as 17,000 K (whereas T_{eff}=10,000 K).

Praderie et al. (1986) and Catala et al. (1986b) report a modulation of the Mg II resonance lines at 2800 Å, which are formed in the wind, with a period of 45 hrs, and of the Ca II K line, formed near the photosphere at the base of the wind, with a period of 32 hrs. These periodic variations were interpreted in terms of rotational modulation by these authors. In their model, a surface magnetic field creates an alternation of fast and slow streams in the wind, thus leading to a periodic modulation of the lines formed in the wind with the star's rotation period. The difference between the period in the Mg II line variations and that of the Ca II K line is difficult to understand in the framework of this model. It was tentatively attributed by these authors to the fact that these lines are not formed at the same distance from the star: the Ca II K line, formed very close to the photosphere, is modulated by the star's rotation, while the Mg II lines, formed much further out in the wind, are modulated by the rotation of the envelope at that distance.

Recent observations with the GHRS onboard the HST by Bouret et al. (1997) have revealed the presence of N V resonance lines near 1240 Å. These lines indicate temperatures above 100,000 K. These authors show that they can be formed within the co-rotating interaction regions which are expected at the interface between fast and slow streams, and which may also be responsible for the observed X-ray flux (Zinnecker & Preibisch, 1994). An interesting alternative to this interpretation would involve a magnetically confined wind as suggested for the Ap star IQ Aur by Babel & Montmerle (1997): the N V resonance lines and the X-ray emission would originate from a post-shock region in the magnetic equatorial plane where magnetically channelled streams from the two hemispheres collide.

The Hα line of AB Aur was also reported to vary from a type II P Cygni profile to a single-peak emission profile (Beskrovnaya et al. 1991, 1995). The most attractive model to explain this type of behavior is that of Pogodin (1992), involving an equatorial wind. In this model, the wind is confined to equatorial regions by a magnetic field, with a variable opening angle. When the line of sight intercepts the wind region, a P Cygni profile is formed, whereas a single-peak emission is produced when it does not. This model has a lot in common with that of Babel & Montmerle (1997) for IQ Aur.

AB Aur was monitored in the He I 5876 Å line during the MUSICOS 92 campaign. The bad weather experienced during the 1992 campaign prevented us from reaching firm conclusions. However, the data show a spectacular variability of this line (Böhm et al. 1996). Whether the variations are periodic or not could not be firmly concluded on the basis of these data, although they present some indication of a periodicity near 34 hours. A high level of short-term variability is also present in addition to the possible periodic modulation. Finally, some low level variability was also discovered in the photospheric lines of AB Aur during the MUSICOS 92 campaign (Catala et al. 1997). Again, the data were not sufficient to conclude anything on the periodicity of these variations.

Vigneron et al. (1990), then more recently Lignières et al. (1996), have studied the effect of the wind on the internal structure and rotation of Herbig Ae stars. They conclude that the

Table 1. Instrument characteristics

site	telescope	spectro.	detector	resolving power	number of orders	wavelength coverage
Mauna Kea Hawaii	3.6m CFHT	MUSICOS	2048^2 STIS2	35,000	68	410 to 810 nm
McDonald Texas	2.1m	Sandiford	1200×400 Reticon	55,000	26	550 to 670 nm
La Palma Canary Islands	2.5m INT	MUSICOS 2	1024^2 Tektronix	35,000	64	440 to 870 nm
OHP France	1.9m	Elodie	1024^2 Tektronix	45,000	67	390 to 680 nm
Xinglong China	2.16m	Echelle	1024^2 Tektronix	45,000	36	560 to 860 nm

torque exerted by the loss of angular momentum at the star's surface excites 3D turbulence in the sub-photospheric layers. These 3D turbulent motions create a mixing layer, which rotates at a slower rate than the inner regions of the star, and which tends to deepen in a typical time scale of 10^6 years. Now, because the angular momentum loss is highest in the equatorial regions, this effect is maximum at the equator, so that the equator is expected to rotate more slowly than the poles.

Most of the ideas presented above assume the presence of a surface magnetic field, which is responsible for structuring the wind both in latitude and in longitude. In a first attempt using spectropolarimetric techniques, Catala et al. (1993) failed to detect this field, yielding an upper limit of about 1000 G for its intensity. The equipartition field at AB Aur's photosphere being of the order of 100 G, this negative result still left a good margin for the models presented above.

Following these previous results, the goals of the MUSICOS 96 observations of AB Aur were twofold: (i) monitor simultaneously lines formed in the photosphere and in various regions of the wind, in order to obtain constraints on the structure of the photosphere/wind complex; and (ii) attempt a direct detection of a surface magnetic field by Zeeman spectropolarimetry.

3. Observations and data reduction

In this section, we describe the instruments used for the MUSICOS 96 campaign, as well as the reduction procedures followed for the AB Aur data. Table 1 shows the participating sites and gives a summary of the instrumentation used.

All the instruments used during this campaign were cross-dispersed echelle spectrographs. The data obtained at OHP, Hawaii, and La Palma cover a very wide wavelength domain, giving access to many photospheric lines, mainly in the blue, and to several lines formed in the wind and chromosphere, such as He I 5876 Å, Hα, and Fe II 5018 Å. The spectrographs in use at Xinglong and McDonald cover a narrower spectral range, but sufficiently wide to contain all wind and chromosphere lines of interest.

The MUSICOS spectropolarimeter (Donati et al. 1998) was transported to Hawaii to be used on the 3.6m CFHT. This particular instrumental setup is designed for the study of stellar magnetic fields through the measurement of linear (Stokes Q and U) and circular polarisation (Stokes V) Zeeman signatures in line profiles.

In addition to the main sites and instruments cited above, some data were also collected at Ritter Observatory, with the 1m telescope, equipped with an echelle spectrograph. Unfortunately, these few spectra of AB Aur were obtained in poor weather conditions, resulting in low signal-to-noise ratios, and could not be used in the analysis below.

The weather was not particularly good during the MUSICOS 96 campaign, especially in Hawaii. However, due to the redundancy of the longitude coverage achieved for this campaign, the AB Aur observations cover about 200 hours, with a duty cycle close to 80% for the first 100 hours, and approximately 40% for the remaining 100 hours.

Table 2 presents the log of the observations. In this table, 'ohp' stands for Observatoire de Haute Provence, 'mdo' for McDonald Observatory, 'cfh' for Canada-France-Hawaii telescope, 'xlo' for Xinglong, and 'int' for Isaak Newton telescope.

The data obtained from Xinglong, McDonald, and the INT were reduced with the "Esprit" reduction software developed by one of us (Donati et al. 1997). In this method, the position of the echelle orders is automatically detected. The images are corrected for pixel-to-pixel inhomogeneities and blaze function by dividing the images containing the stellar spectra by images of flat-field spectra, after flattening the flat-field frame in the direction perpendicular to the spectrograph dispersion. The signal along the orders of the spectrograms is then extracted using the optimal extraction algorithm (Horne 1986, Marsh 1989). The Th/Ar spectra are extracted by simply summing the data about the central location of each order perpendicularly to the order. The wavelength calibration procedure consists basically in a 2D polynomial fit of thorium and argon lines identified in the spectrum (i.e. both in the direction of the grating dispersion and in the direction of the prism cross-dispersion). All details on this reduction procedure can be found in Donati et al. (1997).

The data obtained at OHP were reduced on-site, using the automatic INTER-TACOS procedure (Baranne et al. 1995).

Finally, the spectra obtained at CFHT with the MUSICOS polarimeter were reduced following a dedicated procedure for extracting Stokes V & I parameters (Donati et al. 1997).

The wavelength scales of the stellar spectra were subsequently transformed to a frame linked to the interstellar Na I D lines present in all of our spectra, by simply setting the measured wavelengths of these lines to their laboratory wavelengths. This procedure allows us to compensate for potential systematic wavelength calibration differences between the sites involved in the campaign. We measured in our spectra an heliocentric ve-

Table 2. Log of the MUSICOS 96 observations: the dates refer to Nov. 1996, the UT times are in decimal hours, and the exposure times are in seconds

site	date	UT	texp	site	date	UT	texp
ohp	18	20.46	2701	mdo	21	4.35	1800
ohp	19	0.31	1501	int	21	4.45	400
ohp	19	0.76	1501	int	21	4.57	400
mdo	19	4.10	1200	mdo	21	4.87	1200
mdo	19	4.45	1200	mdo	21	7.23	900
ohp	19	4.91	1201	mdo	21	7.52	600
ohp	19	5.27	1201	mdo	21	7.72	600
mdo	19	6.68	1100	mdo	21	9.95	800
mdo	19	7.02	850	mdo	21	10.25	800
mdo	19	9.03	850	cfh	21	13.25	600
mdo	19	9.32	600	cfh	21	13.46	600
mdo	19	9.50	500	cfh	21	13.67	600
cfh	19	10.22	720	cfh	21	13.88	600
cfh	19	10.47	720	xlo	21	13.95	1200
cfh	19	10.72	720	xlo	21	17.08	1200
cfh	19	10.97	720	xlo	21	17.67	1800
mdo	19	11.48	600	xlo	21	20.78	1800
mdo	19	11.68	700	int	22	0.33	600
cfh	19	13.20	720	int	22	0.52	600
cfh	19	13.43	720	int	22	0.70	600
cfh	19	13.72	720	int	22	2.40	600
cfh	19	13.97	720	int	22	2.58	600
cfh	19	14.92	720	int	22	2.77	600
xlo	19	16.03	1800	mdo	22	4.08	900
xlo	19	18.53	1800	mdo	22	4.35	750
int	19	21.93	1200	mdo	22	4.58	750
int	19	22.30	1200	int	22	4.68	600
int	20	2.90	1200	int	22	4.87	600
int	20	3.27	600	int	22	5.07	600
int	20	3.47	600	mdo	22	6.43	750
mdo	20	4.12	900	mdo	22	6.67	700
mdo	20	4.40	1100	mdo	22	8.93	700
int	20	5.00	1200	mdo	22	9.15	800
int	20	5.37	300	mdo	22	11.43	800
mdo	20	7.00	1000	mdo	22	11.67	800
mdo	20	7.30	1000	xlo	22	13.98	1800
mdo	20	10.00	1200	xlo	22	14.50	1800
mdo	20	10.37	1800	xlo	22	15.53	1800
xlo	20	15.10	1800	xlo	22	16.03	1800
xlo	20	16.27	2700	xlo	22	17.97	1800
xlo	20	18.35	2700	xlo	22	18.48	1800
ohp	20	19.85	1801	xlo	22	19.60	1800
ohp	20	20.38	1801	xlo	22	20.12	1800
int	20	21.40	600	mdo	23	3.60	900
int	20	21.60	600	mdo	23	3.90	1100
int	20	21.80	600	mdo	23	4.23	1100
int	20	22.00	600	mdo	23	6.90	1100
ohp	20	23.48	1802	mdo	23	7.23	1100
ohp	21	0.02	1801	mdo	23	11.40	1000
int	21	0.18	600	mdo	23	11.68	1000
int	21	0.37	600	ohp	23	20.06	1801
int	21	0.55	600	ohp	23	20.59	1801
int	21	2.70	600	int	23	21.37	600
int	21	2.88	360	int	23	21.57	600
ohp	21	2.97	1084	int	23	21.75	600

Table 2. Log of the MUSICOS 96 observations: the dates refer to Nov. 1996, the UT times are in decimal hours, and the exposure times are in seconds

site	date	UT	texp	site	date	UT	texp
ohp	21	3.28	902	int	23	21.93	600
ohp	23	23.63	1091	int	25	2.35	600
ohp	24	0.03	1081	int	25	2.52	600
int	24	0.15	600	int	25	2.70	600
int	24	0.33	600	int	25	4.33	600
ohp	24	0.37	1081	int	25	4.52	600
int	24	0.55	600	int	25	4.70	600
int	24	0.75	600	int	25	21.38	600
int	24	2.38	600	int	25	21.58	600
int	24	2.58	600	int	25	21.75	600
int	24	2.77	600	cfh	26	9.66	720
ohp	24	3.04	1141	cfh	26	10.03	720
ohp	24	3.39	1141	cfh	26	10.27	720
ohp	24	3.77	1320	cfh	26	10.53	720
xlo	24	15.37	1200	cfh	26	13.32	720
xlo	24	15.72	1200	cfh	26	13.57	720
xlo	24	18.75	1200	cfh	26	13.81	720
xlo	24	19.10	1200	cfh	26	14.06	720
ohp	24	19.75	1142	cfh	27	8.11	720
ohp	24	20.08	903	cfh	27	8.38	720
ohp	24	20.39	1054	cfh	27	8.63	720
int	24	22.72	600	cfh	27	8.87	720
int	24	22.90	600	cfh	27	9.11	720
int	24	23.07	600	cfh	27	9.37	720
int	24	23.25	600	cfh	27	9.61	720
int	24	23.45	600	cfh	27	9.87	720
int	25	2.17	600				

locity of $+16\,\mathrm{km\,s^{-1}}$ for the Na I D interstellar lines, while the star systemic heliocentric velocity is $+21\,\mathrm{km\,s^{-1}}$ (Finkenzeller & Jankovics 1984). The star has a small ($+5\,\mathrm{km\,s^{-1}}$) and constant velocity in the reference frame of the Na I D interstellar lines (Finkenzeller & Jankovics 1984), making them an adequate reference for our work. All the spectra presented in this paper, as well as all the velocities quoted, are in the reference frame of the Na I D interstellar lines.

In addition to these spectra obtained during the MUSICOS 96 campaign, we also used for this analysis two series of spectra obtained previously:

– in December 1991 and January 1992, with the MUSICOS spectrograph mounted on the 2m TBL telescope at Pic du Midi Observatory, France. These spectra were discussed by Catala et al. (1993). In that paper, the emission lines of Fe II and He I were studied, but we come back to them in order to analyze their photospheric lines. These data were reduced with the MUSBIC reduction software described in Baudrand & Böhm (1992).

– in November 1994, with the Elodie spectrograph on the 1.93m OHP telescope. These spectra were used in the analysis of short-term photospheric variations of AB Aur (Catala et al. 1997). We re-analyzed them here with the Least-Square

Table 3. Log of the observations: 1991–1992–1994

site	date	UT	texp (sec)
TBL	Dec. 14, 1991	02:12	3600
TBL	Dec. 14, 1991	21:50	7200
TBL	Dec. 16, 1991	21:30	3600
TBL	Jan. 16, 1992	19:16	3600
TBL	Jan. 17, 1992	20:18	3600
TBL	Jan. 18, 1992	19:44	3600
TBL	Jan. 19, 1992	19:06	3600
TBL	Jan. 23, 1992	23:07	3600
TBL	Jan. 24, 1992	18:54	3600
OHP	Nov. 10, 1994	22:34	3600
OHP	Nov. 10, 1994	23:13	1800
OHP	Nov. 10, 1994	23:45	1800
OHP	Nov. 11, 1994	01:07	1800
OHP	Nov. 11, 1994	01:39	1800
OHP	Nov. 11, 1994	02:12	1800
OHP	Nov. 11, 1994	02:45	1800
OHP	Nov. 11, 1994	03:18	1800
OHP	Nov. 11, 1994	04:06	3600

Deconvolution method, for an easier comparison with spectra of the MUSICOS 96 campaign.

The log of these previous observations is given in Table 3.

4. Results

4.1. Photospheric lines

Three of the five instruments used during the MUSICOS 96 campaign have a wide enough spectral coverage to give access to a large number of photospheric lines: these are the 2 MUSICOS spectrographs (Hawaii and the Canaries), and the OHP Elodie spectrograph. The time coverage provided by these 3 sites is only partial, due to their longitude distribution, and to the bad weather conditions at CFHT and OHP during the campaign. However, some very important conclusions can be drawn from these data.

4.1.1. Mean photospheric profile

We used the Least-Square Deconvolution (LSD) technique (Donati et al. 1997) to analyze the variations of a "mean" photospheric line. In this method, a line pattern function is constructed, containing all the lines supposedly present in the spectrum as Dirac functions, with heights set to the central line depths as calculated by Kurucz's (1979) "SYNTHE" program. The observed spectrum is then deconvolved with this line pattern function, yielding a "mean" photospheric line profile. With this technique, line blends are automatically taken into account when all the lines present in the spectrum are considered. Note that the depth of the resulting "mean" line has no physical meaning, but that time variations of this depth, as well as line profiles can be accurately analyzed with this technique. We used a Ku-
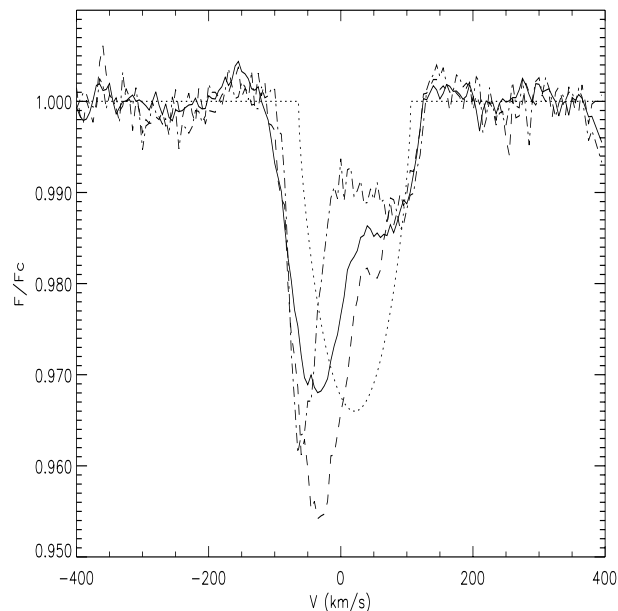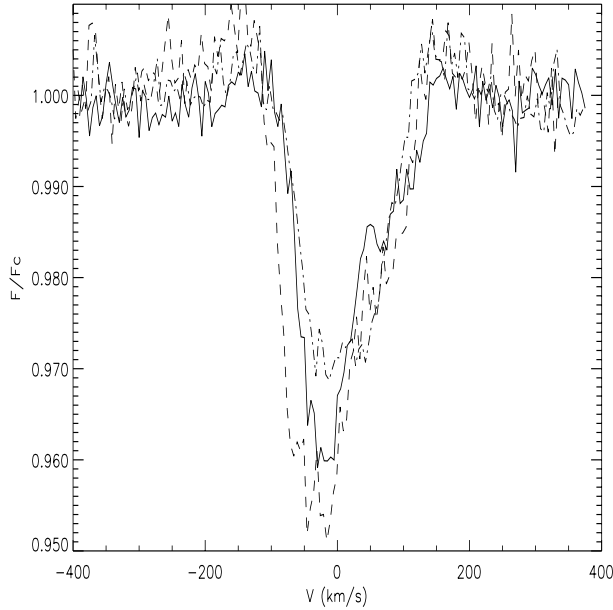

Fig. 1. Some of the mean photospheric profiles of AB Aur. *Full line:* mean profile, averaged over the whole series; *Dashed line:* Nov. 19, 1996, 10.22 UT; *Dashed-dotted line:* Nov. 26, 1996, 14.06 UT; *Dotted line:* Computed rotational profile. All spectra are plotted in the reference frame of the interstellar Na I D lines.

rucz model for $T_{\rm eff} = 10,000$ K and $\log g = 4$, appropriate for AB Aur, for constructing the line pattern function. However, the photospheric spectrum of this star being somewhat peculiar (Böhm & Catala, 1993), we chose to include in the line pattern function only those lines that appear clearly in the high signal-to-noise spectra obtained during this campaign. In addition, we considered only the lines belonging to the common spectral domain of the three cross-dispersed echelle spectrographs used in the campaign. A total of 75 lines were finally used in this analysis. In the following of this work, we shall call "mean" photospheric line, the line constructed with the LSD technique, while the adjective "average" will be reserved for time averages of line profiles.

The shape and variability of the mean photospheric line profile, revealed for the first time with this level of precision thanks to the LSD analysis, is amazing. Fig. 1 displays the mean photospheric profile, additionally averaged in time over the whole MUSICOS 96 series, compared to two examples of individual profiles taken from the campaign. All the mean photospheric profiles obtained during the campaign are highly asymmetric, with a blue side deeper than the red one. We note that the red edge of the line is roughly constant over the whole series, while the blue edge moves back and forth, and the shape of the central parts of the line is highly variable.

The basic characteristics of the photospheric lines are the same in the 1991–1992–1994 spectra, a sample of which is displayed in Fig. 2, and compared with one typical spectrum of the 1996 series, computed using the same lines in the LSD procedure. The same kind of asymmetry is present. We also note that the red edge of the line tends to vary less than the blue

Fig. 2. Some of the mean photospheric profiles of AB Aur observed in 1992, 1994 and 1996. *Full line:* Nov. 19, 1996; *Dashed line:* Jan. 18, 1992; *Dashed-dotted line:* Nov. 10, 1994; All spectra are plotted in the reference frame of the interstellar Na I D lines. The Nov. 19, 1996 spectrum was computed with the same photospheric lines as the 1992–1994 spectra.

and the central parts of the line, not only in the sample spectra presented in Fig. 2, but in all spectra of the 1991–1992–1994 series. Finally, we see that the short-term variations of the line in 1996 are at least as large as the long-term variations between 1991 and 1996.

As a first tentative conclusion of these basic characteristics of the photospheric line, we suggest that the blue side and central parts of the line are formed in regions of the photosphere that have peculiar temperature and/or velocity patterns. The red edge of the line, essentially constant throughout the MUSICOS 96 campaign, and on the longer term between 1991 and 1996, either reveals unperturbed regions of the photosphere, or corresponds to a quasi-permanent and constant accretion onto the stellar photosphere.

Using a sample of the strongest photospheric lines from spectra obtained in Dec. 91, Böhm & Catala (1993) concluded that AB Aur's photospheric spectrum was that of a normal A0V star, and determined a projected rotation velocity of $80 \pm 5 \, \text{km s}^{-1}$.

Catala et al. (1993) also presented one spectrum, obtained on Jan. 21, 1991, where the Fe II 5018 Å line (multiplet 42) appears in absorption and symmetrical, while in all other spectra of AB Aur this line is purely in emission and highly asymmetric. On that occasion the profile of this line was quite compatible with a normal A0V photosphere with a projected rotation velocity of $80 \, \text{km s}^{-1}$, in agreement with the value determined by Böhm & Catala (1993), and a stellar heliocentric radial velocity of $21 \, \text{km s}^{-1}$, confirming the value measured by Finkenzeller & Jankovics (1984) using the higher Balmer lines.

We must then conclude that the $v\sin i$ value of AB Aur cannot be much higher than $80 \, \text{km s}^{-1}$.

On the other hand, with the LSD method used here, we find that the mean photospheric line is always asymmetric and wider than a standard rotational profile of $80 \, \text{km s}^{-1}$, not only in our data of the 1996 MUSICOS campaign, but also in the re-analyzed data of 1991, 1992 and 1994. A projected rotational velocity of the order of $140 \, \text{km s}^{-1}$ would be necessary to reproduce the red edge of the line. Such a high value for $v\sin i$ would be inconsistent with many of the spectra obtained during the 1991, 1992 and 1996 campaigns, which are narrower, with the profiles of the strong photospheric lines used in Böhm & Catala's analysis, and with the profile of the Fe II 5018 Å line of Jan. 21, 1991.

We cannot invoke a value of the star's radial velocity much higher than $21 \, \text{km s}^{-1}$, as it would be inconsistent with both Finkenzeller & Jankovics's measurements, and the Fe II 5018 Å line of Jan. 21, 1991. We also note that Finkenzeller (1983) concluded that AB Aur was not a member of a multiple system, so that we do not expect significant changes in its radial velocity.

Thus, in order to make the red edge of the mean photospheric line in our 1991, 1992, 1994 and 1996 data consistent with the previously determined values of $v\sin i$ and the radial velocity, we need to assume

- either a quasi-permanent and constant accretion onto the stellar photosphere;
- or no accretion, but a broader local profile for the line through turbulent motions, with velocities of the order of $40 \, \text{km s}^{-1}$.

Turbulent velocities as high as $45 \, \text{km s}^{-1}$ were deduced in the wind of AB Aur (Catala & Kunasz 1987), and even higher values of the turbulent velocities in the wind are needed to account for the shape of the newly discovered N V resonance lines (Bouret et al. 1997). It seems clear that the variable parts of the photospheric lines (central and blue parts), which are likely to be partly formed at the base of the wind, may also be affected by strong turbulent motions. In the hypothesis discussed here, we also need strong turbulent motions in the unperturbed layers of the photosphere. However, we do not have any other independent evidence for such motions in the unperturbed photosphere, except that a high level of turbulence in the photosphere is predicted by the model of Lignières et al. (1996), which includes a mixing layer.

For the following analysis, we will therefore pursue the former hypothesis, assuming a non-turbulent photosphere with a projected rotation velocity of $85 \, \text{km s}^{-1}$, which is the upper limit derived by Böhm & Catala (1993). We note however that most of the conclusions presented below concerning the time variability of the photospheric lines do not depend much on the choice of the basic photospheric profile.

A photospheric rotational profile computed with the assumption cited above is also shown in Fig. 1, plotted in the IS Na I D line reference frame (i.e. shifted by $5 \, \text{km s}^{-1}$ with respect to the stellar rest frame). The depth of the computed profile was
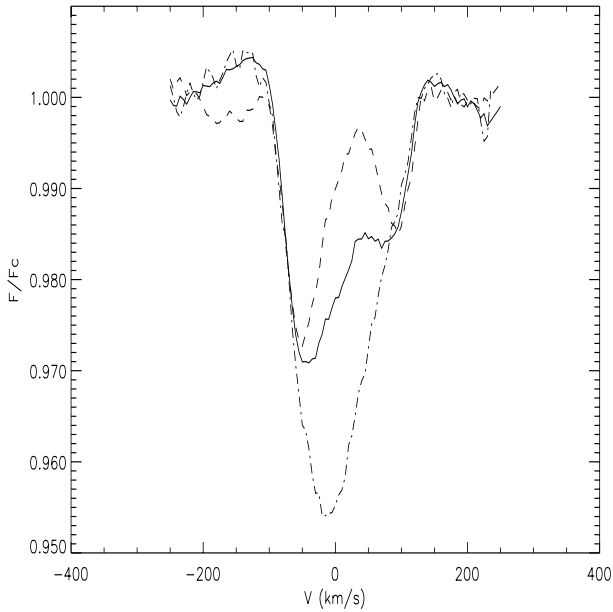
Fig. 3. Comparison of various averages of photospheric profiles. All profiles were averaged over all spectra obtained at CFHT during the campaign. The different curves correspond to different choices of lines for the Least-Square Deconvolution technique. *Full line:* all photospheric lines; *Dashed line:* only Fe II lines; *Dashed-dotted line:* only strong lines of Si II, Mg II, O I.

Fig. 4. The standard deviation across the photospheric line profile, for the whole series (full line), divided at each velocity by the mean photospheric line profile, averaged over the whole series. The mean-average profile, properly translated and rescaled to fit in the figure, is given for reference (dashed line)

adjusted in order to reproduce correctly the shape of the mean photospheric line of a reference A0V star, HR 3314, calculated with the LSD method using the same lines as for AB Aur.

We also find that the shape of the mean photospheric line depends significantly upon the choice of lines used in the averaging procedure of the LSD method. We have computed the average photospheric line, using lines of Fe II, Fe I, Cr II, Mg II, O I, Ti II, and Si II, as well as choosing only lines from neutral species, or only lines of singly ionized species, or only strong lines. These various mean lines differ from each other. Fig. 3 presents an example of this behavior, and displays the mean photospheric profiles obtained with all lines, with only those of Fe II, and with only the strong lines of Si II, Mg II and O I. These results must be manipulated with care, as the LSD analysis is subject to line blending when only line subsets are considered. Before applying the LSD algorithm to particular line subsets, we carefully examined the potential presence of strong blends, and removed from the list lines which could suffer from such blends. Also, in order to optimize the final number of lines considered, we used only the spectra obtained at CFHT for this part of the analysis, as they provide the widest spectral domain. The results show that the mean profile obtained with only strong photospheric lines is much more symmetrical than that computed with all lines, probably because of the saturation of strong lines. On the contrary, Fe II lines seem to depart much more from a symmetrical profile. In particular, they show a very prominent emission in the central and red parts of the line, at the same velocity where we see a flux plateau in the mean photospheric profile computed with all available lines. We have checked that
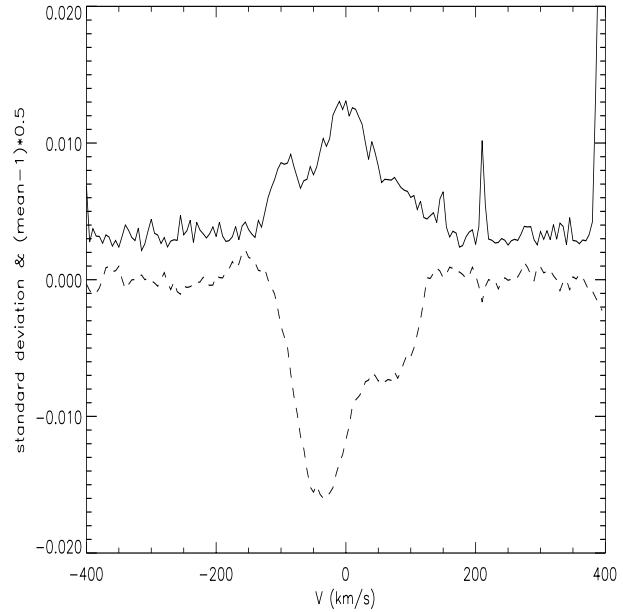
the behavior of the Fe II lines described above is representative of that of all moderate and weak lines in the spectrum of AB Aur. It seems clear that the phenomenon responsible for the departures from pure unperturbed photospheric profile affects the formation of most lines, rather than simply the adjacent continuum, as in the case of dark spots. It is quite reasonable to conclude from the remarks above that at least part of the observed line asymmetries are due to the presence in the stellar atmosphere of hot gas overlying some areas of the photosphere.

4.1.2. Photospheric line dynamical spectrum

From this point on, we will refer only to the mean photospheric line obtained with the LSD technique using all the photospheric lines present in the spectrum.

Fig. 4 presents the standard deviation across the line profile for the whole series, divided at each velocity by the mean photospheric line profile, averaged over the whole series. This procedure allows us to examine the relative variations of the line profile and to compare these relative variations in the different parts of the line. It can be readily checked that the line variations are real, with a main peak near zero velocity, and a secondary peak near $-80\,\mathrm{km\,s^{-1}}$, corresponding to the blue side of the line. The maximum standard deviation in the line reaches 1.3%, while the standard deviation in the continuum adjacent to the line, giving a measure of the noise level, is only of the order of 0.3%.

We then subtracted, from each profile in the series, the rotational profile computed with the assumption of a non-turbulent phostosphere with $v\sin i$=85 km s^{-1}. The resulting dynamic im-

age is displayed in Fig. 5. The residuals show almost systematically a blue absorption component, an emission component slightly redward of line center, and a red absorption component. In the following, we shall call red component the emission component which is slightly redshifted, and red edge component the redmost component appearing in absorption. A modulation of the blue component is clearly suggested, with a period near 30 hours, while no clear modulated displacement of the red and redmost components can be seen. The red component is redshifted by 25 km s^{-1} on average, while the redmost component shows a mean redshift of 95 km s^{-1}. We detect strong changes in the intensity of the red emission component, which are primarily responsible for the variations in the equivalent width reported in Sect. 4.1.4.

The redmost absorption component, which is constant in velocity, may reflect the fact that the baseline rotational profile that was subtracted from each one of the spectra does not correspond to the real underlying photospheric spectrum. This would be the case for instance if some high level of photospheric turbulence was present in AB Aur. Although, as argued earlier, we have no decisive evidence for such supersonic turbulence in the photosphere, we consider that the existence of this redmost absorption component is doubtful, and do not discuss it in detail in the rest of this paper.

In order to quantify the modulations displayed by the dynamical spectrum displayed in Fig. 5, and as a first step of a systematic analysis of these variations, we performed a period search across the photospheric line, in the following way. The line was divided into velocity bins 25 km s^{-1} wide, and a periodogram of the line intensity averaged over 25 km s^{-1} was calculated for each one of these bins. The periodogram is defined as:

$$1 - R = 1 - \sum \left[y_i - f_i \right]^2 / \sum y_i^2 \qquad (1)$$

where the y_i are the data points, i.e. the intensity in the line after subtraction of the rotating profile, averaged over bins 25 km s^{-1} wide, and the f_i the values of a fitting sine wave, computed for each trial period with the amplitude and the phase as free parameters. Such a periodogram is equivalent to the more classical Scargle (1982) periodogram, and has the additional advantage of providing an estimate of the phase and amplitude of the potential periodic variations. We constructed this periodogram, calculating $1 - R$ for a set of 500 trial periods, ranging from 20 to 70 hrs.

Fig. 6 presents the result of this period analysis. If we except the peaks occurring at periods shorter than 28 hrs, dominated by the aliases produced by the gaps in the photospheric data, and the signal arising at very long periods, whose origin is uncertain, we find that the most prominent features in the part of this periodogram corresponding to the velocity range spanned by the photospheric line, are three major peaks, located at the velocities of the three components identified on the dynamical spectrum of Fig. 5: the slightly redshifted component and the red edge of the line exhibit two distinct peaks, both with a period near 43 hrs, while the third peak in the periodogram, corresponding to the blueshifted component, appears near 37
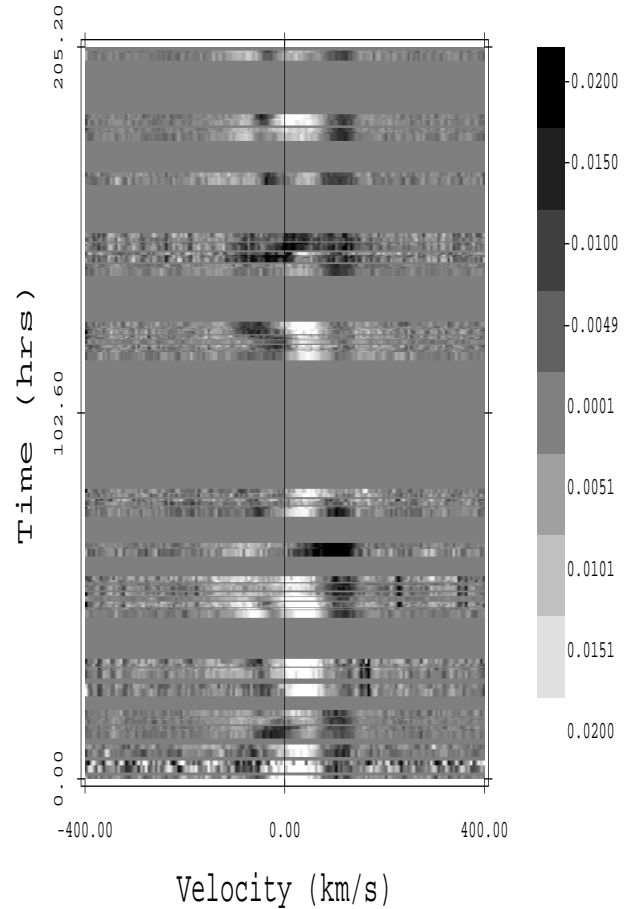

Fig. 5. Residuals after subtracting a rotation profile from the series of photospheric profiles of AB Aur. The spectra are in the reference frame of the interstellar Na I D lines. A $v\sin i$ of 85 km s^{-1}, and a radial velocity of 5 km s^{-1} with respect to the interstellar Na I D lines, corresponding to a stellar heliocentric radial velocity of 21 km s^{-1}, were assumed for the computed rotation profile. The origin of time is Nov. 18, 1996, 20.46 UT. The height of each spectrum does not correspond to the actual duration of the corresponding exposure, but has been increased for display purposes. The grey-scale coding is indicated on the right side of the figure: dark shading corresponds to negative values, while light shading corresponds to positive values.

hrs. The two periods detected in this periodogram (37 and 43 hrs) appear significantly different. These results indicate that the variations of the photospheric line contain significant periodic components, but also suggest clearly different behaviors of the blue and red sides of the line. This first and natural attempt at analyzing the periodicity present in the mean photospheric profile motivated a more detailed investigation, which is presented below.

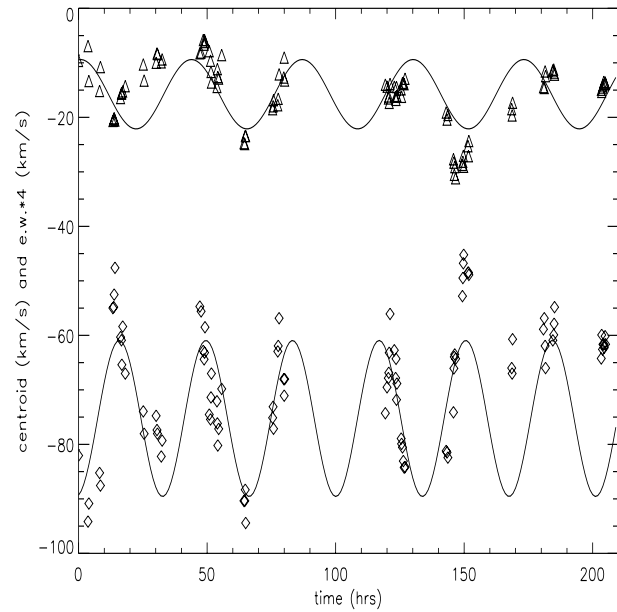### 4.1.3. Components of the mean photospheric line

Guided by these results, we studied separately the three components appearing in the mean photospheric line after subtraction of the computed rotational profile introduced earlier. In each spectrum of the series, we identified "by eye" each one of these
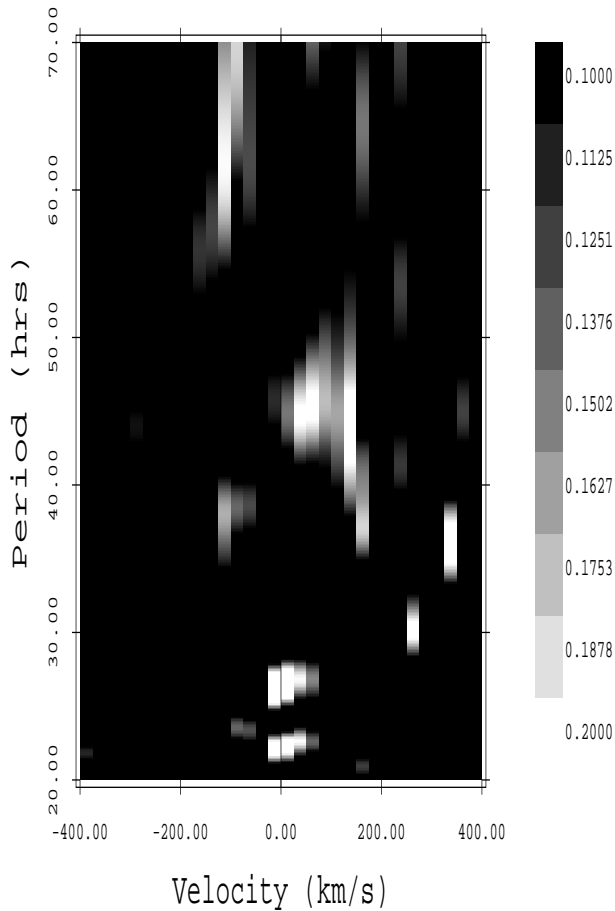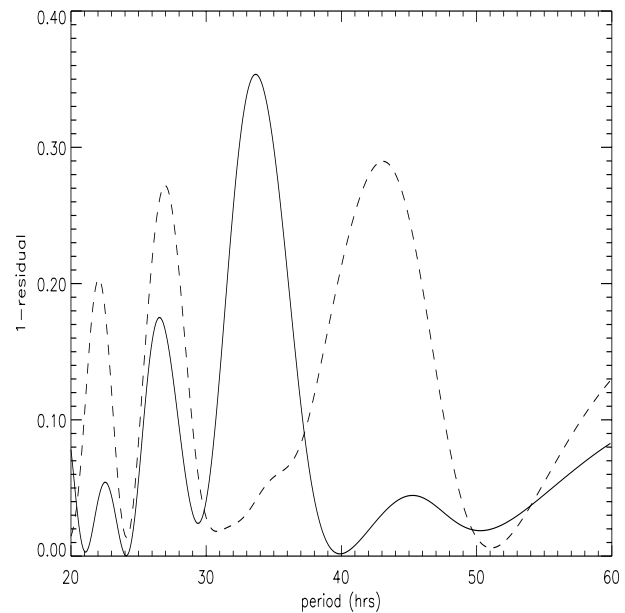
Fig. 6. Two-dimensional period analysis of the mean photospheric line. The periodogram is calculated according to Eq. (1). Most features with periods shorter than 28 hrs are mainly due to aliases produced by the gaps in the data.


Fig. 7. The time variation of the centroids of the blue absorption component (diamonds) and of the total equivalent width (triangles) of the average photospheric line. Note that the equivalent width is multiplied by 4 in this plot for display purposes. Best fit sine waves, with periods of respectively 33.7 and 43.1 hrs, are also indicated (full lines).

Fig. 8. Periodogram of the variation of the centroid of the blue component (full line) and of the total equivalent width (dashed line) of the mean photospheric line. For each trial period, we plot $1 - R = 1 - \sum [y_i - f_i]^2 / \sum y_i^2$, where the y_i are the data points and the f_i the values of the fitting sine wave.

components, fitted it by a gaussian, and determined its centroid, intensity and width. The most interesting result of this analysis is displayed in Fig. 7, which shows the centroid of the blue component as a function of time. This component has a radial velocity modulated between $-100 \, \text{km s}^{-1}$ and $-40 \, \text{km s}^{-1}$.

The centroid of the blue component indeed seems periodically modulated. In order to quantitatively test this hypothesis, we computed a periodogram for the time series corresponding to this centroid, with the same method as described earlier Eq. (1). The best result is obtained when the last few data points (after t=160 hrs) are given a zero weight in the fitting, as there appears to be a strong change in the variability pattern around that time. The periodogram is displayed in Fig. 8, and indicates that the variations of this centroid are modulated with a period near 34 hrs. Using the definition of the periodogram given by Scargle (1982) instead of Eq. (1) (Scargle has demonstrated that the two approaches are equivalent), and applying the statistical analysis presented in that paper, we find a false alarm probability (i.e. the probability that this 34 hr peak is due to noise) of the order of $4 \, 10^{-7}$ for our 500 trial period periodogram. The width of the corresponding maximum in the periodogram

gives us a rough estimate of the error bar on this period. We find $P = 33.7 \pm 2.5$ hrs. This period is close to, and in any case within the error bar of, that found by Catala et al. (1986b) for the Ca II K line of AB Aur (32 ± 4 hrs). It is also consistent with the peaks corresponding to the blue component in the two-
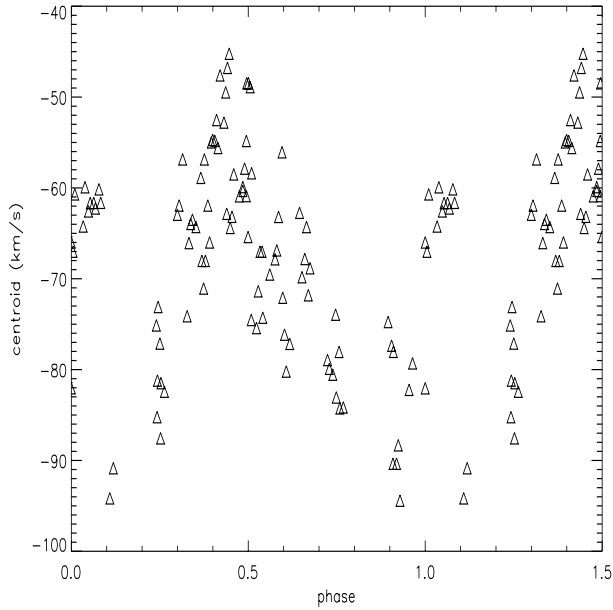
Fig. 9. Centroid of the blue component of the average photospheric line, rephased with a period of 33.7 hrs.

dimensional periodogram of the intensity in the photospheric mean profile, presented in Fig. 6. The sine wave fit corresponding to the highest peak in the periodogram (period: 33.7 hrs) is plotted in Fig. 7, to be compared to the time variation of the centroid of the blue photospheric component. The data, rephased with the 33.7 hr period, are shown in Fig. 9. The modulation is obvious on this figure, the data points at $V = -60\,\mathrm{km\,s}^{-1}$ near phases 0 and 1, which are the only ones departing from the modulation, corresponding to intervals of time after t=160 hrs, when the variability pattern obviously has changed. We also checked that replacing our data by a random time series produces no signal in the periodogram near 34 hrs. Figs. 6, 7, 8 & 9 convincingly demonstrate that the blue component velocity is indeed modulated with this period, although a certain level of additional variability is present on top of the strictly periodic modulation. The other two peaks appearing in the periodogram (near 22 and 26 hrs) are not real, but related to the gaps in our data set. We find that they still appear in the periodogram of a pure sine wave with period 33.7 hrs, restricted to the same time coverage as our data.

Compared to the variations of the blue component velocity, the red emission and redmost absorption components do not appear variable in velocity. The red component radial velocity is constant except at times when the blue absorption component is near its reddest location. It is not clear if the small variations measured in the red component velocity, ranging between 10 and $30\,\mathrm{km\,s}^{-1}$ with an rms dispersion of $10\,\mathrm{km\,s}^{-1}$, are real or simply reflect the fact that the blue absorption component is sometimes eating up the blue edge of the red component, thus resulting in an apparent redshift of the latter. The redmost absorption component is even more constant in velocity, with an rms dispersion of only $4\,\mathrm{km\,s}^{-1}$.

4.1.4. Variations of the photospheric line equivalent width

The total equivalent width of the mean photospheric line is highly variable, with an rms variation of $1.5\,\mathrm{km\,s}^{-1}$, i.e. 38% of its average value. We find that these variations, displayed in Fig. 7, present some regularity, including a seemingly periodic modulation. We note that these variations are primarily due to the red component, but the measurement of the intensity of this component alone is extremely difficult, and we have preferred to present the time variation analysis of the total equivalent width instead, which on the contrary is straighforward to measure.

As shown in the 2D periodogram of the intensity in the mean photospheric line presented in Fig. 6, the modulated component of these variations is mainly due to the red components of the line. A periodogram analysis of the equivalent width variations, similar to that performed on the centroid velocities, indicates that a 43.1 hr period may be present in the modulated component of these variations. This periodogram is shown in Fig. 8. This period is significantly distinct from the one we see in the velocity variations of the blue component, in agreement with the results of the 2D intensity periodogram of Fig. 6. As expected, the additional spurious peaks near 22 and 26 hrs, due to data gaps, are also present in this periodogram. However, a close inspection of Fig. 7 reveals that the 43.1 hr period found in the analysis is primarily due to two deep minima in the equivalent width near t=65 hrs and t=150 hrs. The periodicity of the equivalent width variations is therefore unclear, and the peak in the corresponding periodogram, as well as the corresponding peaks displayed by the 2D intensity periodogram of Fig. 6, may be fortuitous. Clearly, additional data would be required to check this point.

4.2. Search for circular polarization in the photospheric lines

The MUSICOS spectropolarimeter was used on the 3.6m CFHT for this campaign, in the hope of detecting directly a surface magnetic field in AB Aur, through the measurement of circular polarization Zeeman signatures in the line profiles. However, the seeing and transparency conditions experienced at Mauna Kea during the campaign were particularly bad, and the signal-to-noise ratios obtained in our spectra did not meet our expectations, by a large factor.

No signal was detected in the spectra of the V Stokes parameter for the average photospheric line, in any of the AB Aur spectra obtained with the instrument. The final 1-σ upper-limit for the strength of a net radial field in a magnetic region covering 2.5% of the total stellar surface, and facing the observer, would be of the order of 300 G.

4.3. The He I D3 line

The He I 5876 Å line most often appears in emission in AB Aur, as shown by Böhm et al. (1996). The spectacular variability exhibited by this line during the MUSICOS 92 campaign, as well as the indication that this variability may have a strong periodic component, motivated us for choosing it as the center of the
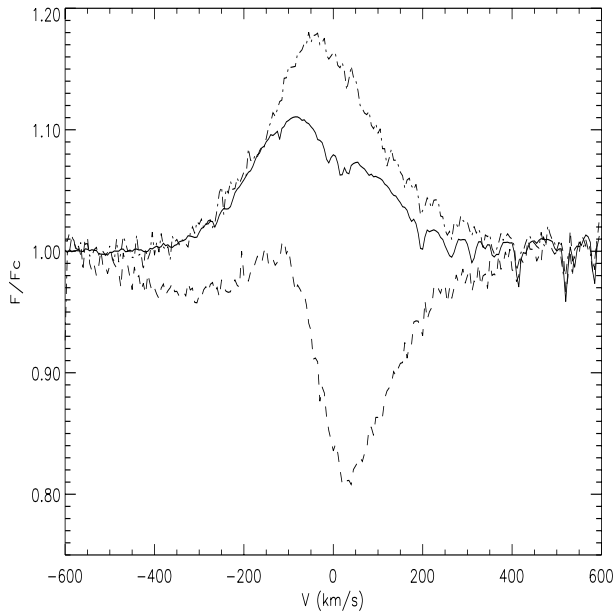
Fig. 10. Some of the He I D3 profiles of AB Aur. *Full line:* mean profile, averaged over the whole series; *Dashed line:* Nov. 21, 1996, 17.67 UT; *Dashed-dotted line:* Nov. 26, 1996, 14.06 UT; the sharp lines predominantly appearing on the red side of this plot are telluric water vapour lines

Fig. 11. The standard deviation across the He I D3 line profile, for the whole series (full line), divided at each velocity by the average line profile. The average profile, properly translated and rescaled to fit in the figure, is given for reference (dashed line); the small peaks on the red side of the plot are due to telluric water vapour lines.

MUSICOS 96 campaign. Therefore, all instruments involved in the campaign observed this line in the best possible configuration. As a result, the time coverage obtained on this line is better than that of the photospheric lines.

As in 1992, the variability of this line is amazing. Fig. 10 shows the mean profile for this line, averaged over the whole series, with two individual mean profiles showing the high level of variability. A quantitative measure of variability across the line is obtained by computing the standard deviation in each velocity bin and dividing this by the average flux in this velocity bin. The result of this analysis is displayed in Fig. 11.

4.3.1. Dynamical spectrum of the He I D3 line

A dynamic spectrum of the He I D3 line is presented in Fig. 12. The variability of the central part and red side of the line is in great part due to a single dramatic event, around t=65 hrs, when a deep and broad absorption appears on the red side and in the central part of the line. One of the spectra obtained during this event is presented in dashed line in Fig. 10. This phenomenon repeats itself, although with lower amplitude, near t=170 hrs. This event is reminiscent of a similar one, observed during the MUSICOS 92 campaign, with the same characteristics.

In addition to these strong events, we also note a strong variability present all along the series, as in 1992, with the following characteristics:

– The line has 2 separate components, one blue and one red, which can be easily identified in the average profile displayed as a full line in Fig. 10.

– The blue component is always in emission. Its centroid varies in velocity, and its amplitude is also variable.
– The red component is most often in emission, but appears in absorption on several occasions, including during the dramatic event mentioned previously. Its centroid does not change significantly, but its intensity is highly variable.

We calculated a 2D periodogram of the He I line intensity averaged over velocity bins of 25 km s^{-1}, with the same period analysis method as applied to the photospheric lines, exploring 500 trial periods between 20 and 70 hrs. The result is displayed in Fig. 13, and clearly shows two separate peaks, corresponding respectively to the blue and the red components described above, appearing at the same period near 43 hrs. Note that, the time coverage of this series being much better than that of the photospheric lines analyzed earlier, this periodogram does not show any feature at short periods as the one of photospheric lines did.

We have therefore separated the analysis of both components, and this further investigation is presented below.

4.3.2. Components of the He I D3 line

Each profile in the series was fitted by a sum of 2 gaussians. This fitting procedure is very satisfactory, and the line can be successfully fitted by these 2 independent gaussians at most times during the campaign. However, the solution of the fitting is definitely not unique when the 2 components occur at similar velocities (leading to an almost symmetrical broad profile for the He I D3 line). Our automatic procedure will systematically choose two separate components, with moderate widths, rather
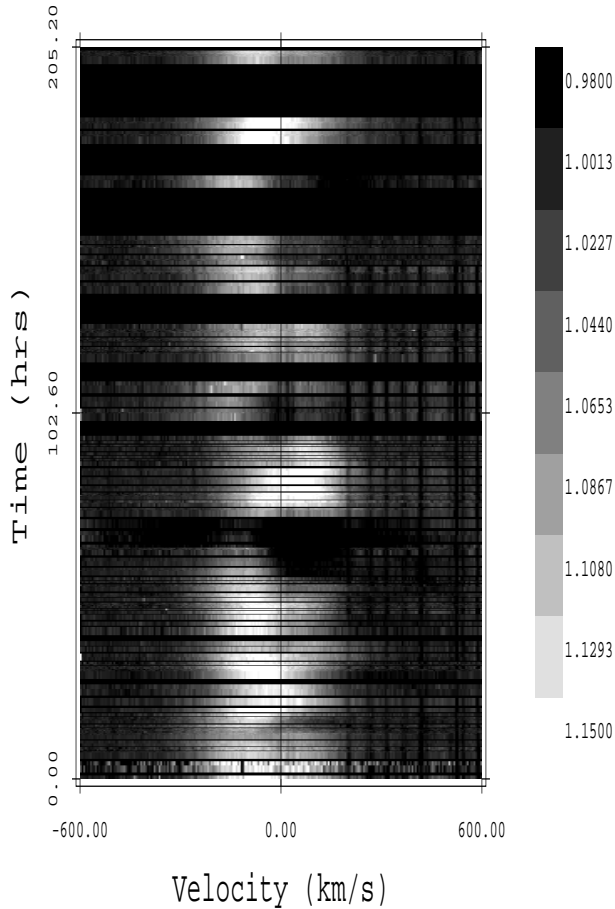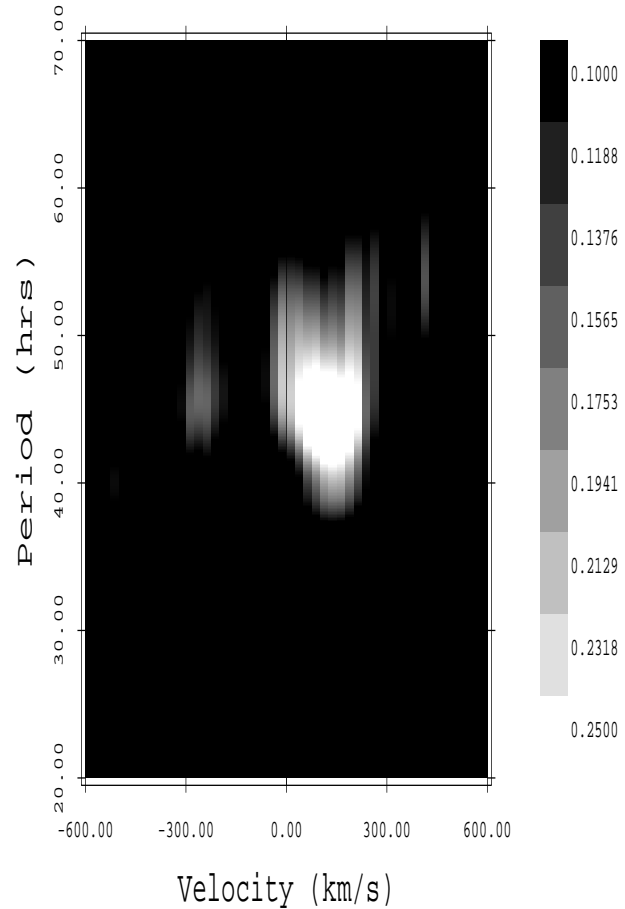
Fig. 12. Dynamic spectrum of the He I D3 line. The height of each spectrum does not correspond to the actual duration of the corresponding exposure, but has been increased for display purposes.
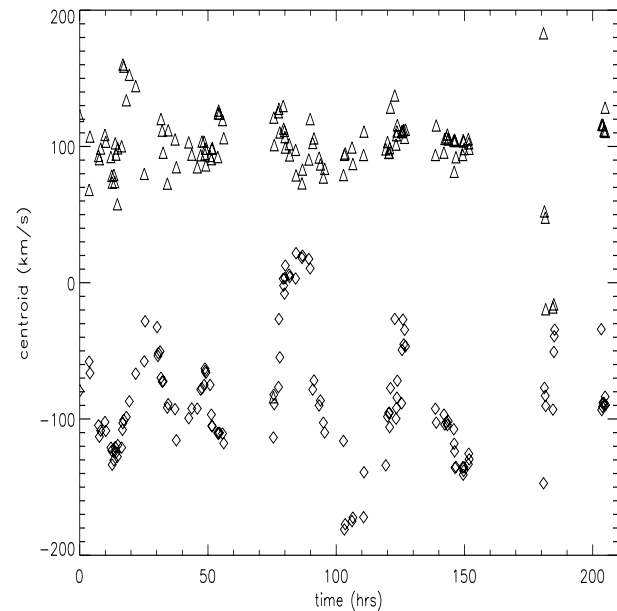

Fig. 13. Two-dimensional period analysis of the He I D3 line. The periodogram is calculated according to Eq. (1).

Fig. 14. The time variation of the centroids of the blue (diamonds) and red (triangles) components of the He I D3 line. The data points near t=65 hrs and t=170 hrs, corresponding to the strong absorption events discussed in the text, are omitted. None of the two data sets has been shifted in this figure.

than two wider components at the same velocity. We must keep this caveat in mind when discussing the results, and consider that the blue component can be somewhat redder than determined when it approaches the line center, while the red component can be bluer. Furthermore, the automatic procedure also leads to spurious results concerning the centroid of the blue component during phases when the red component appears strongly in absorption, i.e. near t=65 hrs and t=170 hrs.

Fig. 14 presents the centroids of these 2 gaussians as a function of time. Note that we have omitted the data points corresponding to phases when the red component is in absorption, near t=65 hrs and t=170 hrs, because of the problems mentioned above. It can be verified that the centroid of the red component is much less variable than the blue one. In fact, the centroid of the red component is more or less constant all through the campaign, except near t=180 hrs. The strong variation of this component is therefore primarily due to dramatic changes in intensity without much velocity variation.

The variations of the blue component centroid occur on a shorter time scale between t=0 and t=65 hrs than after t=65 hrs. A periodic modulation with a period near 45 hrs is suggested in the series after t=65 hrs, whereas a period twice as short seems

to prevail between t=0 and t=65 hrs. Note that the moment when the double wave is changed into a simple wave coincides with the dramatic absorption event described earlier.

We applied to these data the same period search method as used in the case of photospheric lines. The results are presented in Fig. 15. We find a clear maximum of the periodogram near 45 hrs. Applying the same statistical analysis as for the photospheric line variations, derived from Scargle (1982), we find a false alarm probability near $1.5\,10^{-17}$ for this period in our 500 trial period periodogram. The corresponding peak in the periodogram is rather wide, and indicates a period $P = 45^{+10}_{-3.5}$ hrs. This error bar, although it is wide, does not include the 34 hr period derived for the variations of the blue component of the mean photospheric line.

Fig. 16 presents the data rephased with a period of 45.1 hrs (period giving the best sine wave fit), plotting separately for the first and second halves of the data. We note that the data of the second part of the campaign (after t=65 hrs) are indeed consistent with a simple periodicity with P=45.1 hrs, while those of the first part of the campaign (before t=65 hrs) are distributed on a double wave in the phase diagram calculated with the same period. However, this conclusion is weakened by the fact that we see the double-wave for only 1.5 times the period. It may be worth to note that this double wave is not symmetric, which could be interpreted in terms of the presence of two different structured areas almost opposite to each other, one of which would disappear after 65 hrs.

Finally, we find no correlation between the variations of the centroid of the blue component of the He I line and those of the blue component of the mean photospheric line.

### 4.3.3. Variations of the equivalent width of the He I D3 line

In addition to the results presented above, we measure strong variations in the total equivalent width of the He I D3 line, with an rms dispersion of $20\,\mathrm{km\,s^{-1}}$, i.e. 56% of its mean value. The variations are dominated by the red half of the line, from line center redward, for which the rms dispersion is 100% of the average equivalent width. However, the measurements of the equivalent width of the He I line blue and red components are made difficult by the cross-talk between the two components that we have mentioned previously, and we have preferred to analyze the total equivalent width of the line, which is a more reliable and easy to measure quantity.

The variation of the total equivalent width reaches 200% during the absorption event at t=65 hrs. Fig. 17 displays these variations, compared to those of the equivalent width of the mean photospheric line during the campaign. We notice that the two data sets are correlated, with a correlation coefficient of 0.70. This correlation is shown in Fig. 18.

The variations of the equivalent width of the He I D3 line seem to be modulated with the same period as those of the centroid of the blue component, as shown in Fig. 15. The false alarm probability of the corresponding peak in the periodogram is $2.4\,10^{-6}$. This period, near 45 hrs, is also close to that displayed by the equivalent width of the photospheric lines, whose
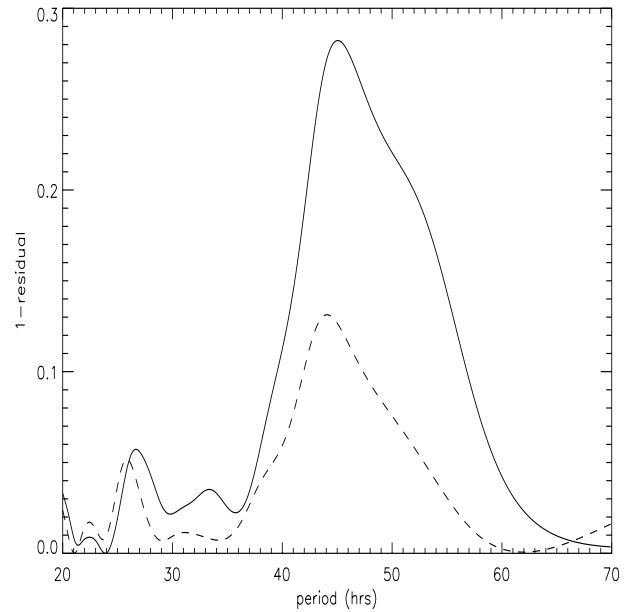

Fig. 15. Periodogram of the centroid of the He I D3 blue component (full line) and of the line total equivalent width (dashed line).
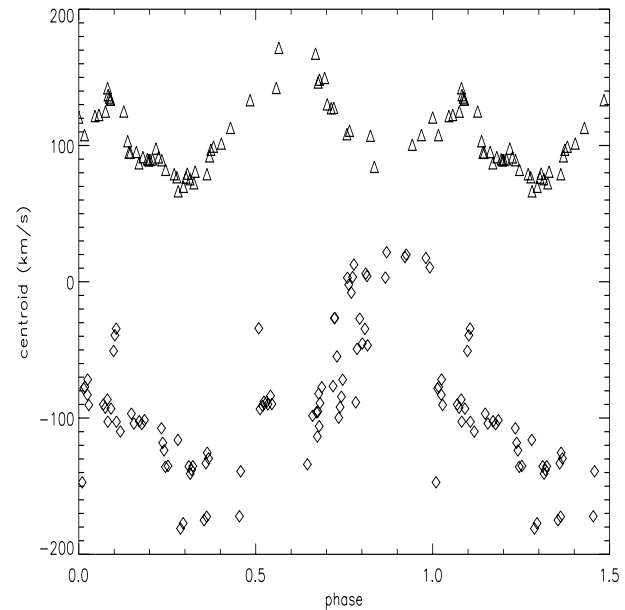

Fig. 16. Centroid of the He I D3 blue component, rephased with a period of 45.1 hrs. The data have been separated in two parts: from t=0 to t=65 hrs (triangles); from t=65 to t=210 hrs (diamonds). The data from t=0 to t=65 hrs are shifted by $+200\,\mathrm{km\,s^{-1}}$ for clarity.

variation is also dominated by the red half of the line. However, while the periodic appearance of the equivalent width variations in the photospheric lines may be fortuitous, due to moderate time coverage of our observations, there seems to be no doubt about the periodicity of the equivalent width of the He I line, which was much better covered by our observations (see Fig. 17). The correlation between these two quantities, shown in Fig. 18, therefore adds some credibility to the 43 hr periodicity found in the photospheric line equivalent width.
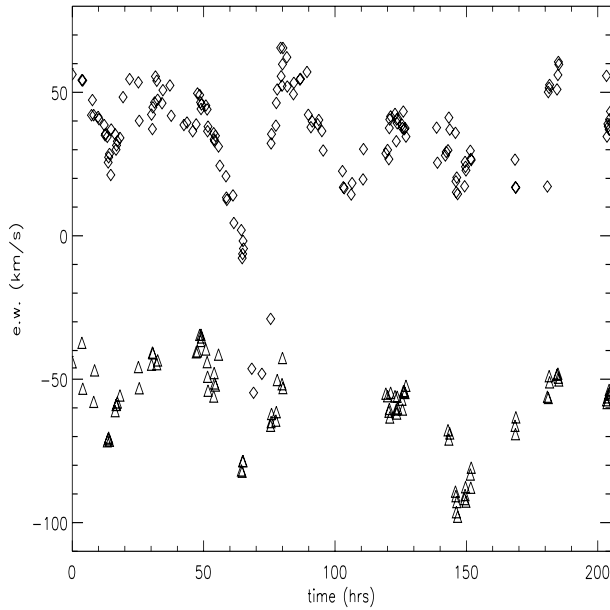
Fig. 17. Equivalent width of the He I D3 line (diamonds) and of the photospheric lines (triangles), as a function of time. The equivalent width for the photospheric lines was multiplied by 10, then shifted by $-20\,\mathrm{km\,s^{-1}}$ for plotting purposes.
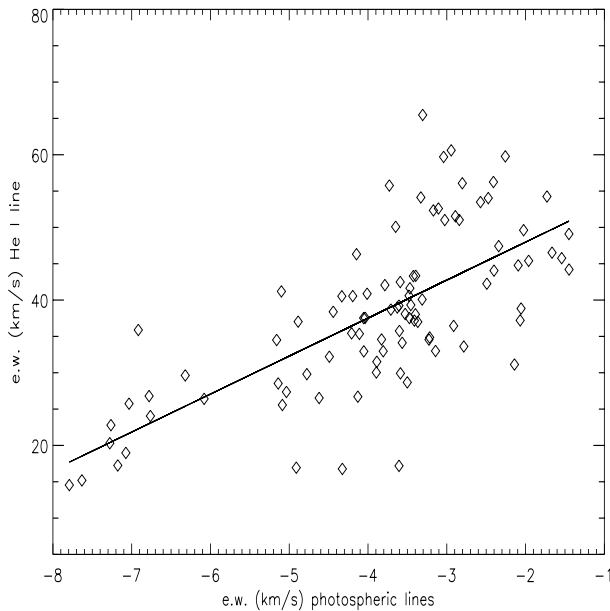
Fig. 18. Correlation between the equivalent width of the He I D3 line (ordinates) and that of the photospheric lines (abscissae). The four most extreme spectra recorded during the strong absorption event described in the text, corresponding to very negative values of the He I line equivalent width, were omitted.

We detect a strong correlation between the centroid of the blue component of the He I D3 line and the total equivalent width of this line, with a correlation coefficient of 0.74. It seems that this correlation is driven by the intensity variations of the red component, which tends to be stronger when the blue component is near zero velocity. However, because of the cross-talk

between the two He I components, we cannot exclude that it simply reflects variations of the blue component intensity accompanying its velocity variations. In this case, both the correlation discussed here and the 45 hr period detected in the total equivalent width variations would be attributable to the blue component alone.

4.4. The Hα line

The Hα line of AB Aur has been observed repeatedly in the past. It appears most often as a type II P Cygni profile, that is with an intense redshifted emission and a blueshifted absorption component. Occasionally, this line exhibits a single component emission and no absorption, or a type III P Cygni profile, i.e. with an additional blueshifted emission component on the blue side of the absorption component (Beskrovnaya et al. 1991, 1995).

We observed the three types of profiles during the campaign. Figs. 19 and 20 give an illustration of the high level of variability of this line. We note that the relative variation of the emission component is much smaller than that of the absorption component. Although a few of our spectra are saturated near the top of the Hα emission component, this strong difference between the levels of variability of the blue and red component of the Hα P Cygni profile is real. In the following, we will discuss mainly the absorption component of the line.

Fig. 21 shows a dynamic spectrum of the line, focussed on the absorption component (the emission component is "saturated" on the scale used for the figure). It can be noted that this component varies in intensity, width, and shape. Fig. 21 suggests no obvious strictly periodic modulation of any part of the Hα line, although dramatic variability is exhibited by its absorption component. The blue edge of the Hα absorption component appears much variable, exhibiting what appears to be a set of partial sinusoids in velocity space, with amplitudes in the range $100–150\,\mathrm{km\,s^{-1}}$, and with timescales of the order of 40–50 hours.

We have systematically looked for periodicity in this line, using a similar 2D periodogram as in the case of photospheric and He I lines, exploring 500 trial periods between 20 and 120 hrs. The result is shown in Fig. 22, and indicates a very complex behavior of this line. We do see some power at a period near 50 hrs, and at a velocity of $-300\,\mathrm{km\,s^{-1}}$, which may be due to a real periodic behavior, although we cannot attach a great level of confidence to this result. The other strong peaks appearing in this 2-D periodogram do not correspond to periodic phenomena, but simply to the occurrence of only two events. In that case the period of a given peak in the periodogram simply measures the time separation between the two occurrences of the event. Thus, the feature seen in Fig. 22 near $-400\,\mathrm{km\,s^{-1}}$ and 70 hrs is related to the widening of the absorption component near t=58 hrs and near t=130 hrs (see Fig. 21). The other strong peak near $-100\,\mathrm{km\,s^{-1}}$ and 90 hrs corresponds to the apparent widening of the emission component near t=40 and t=135 hrs.

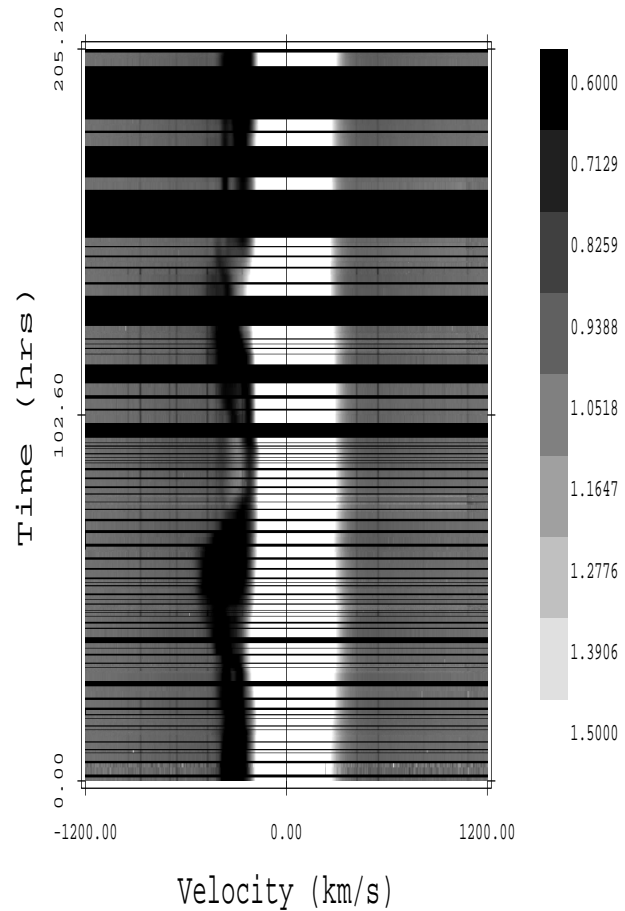We have therefore no strong evidence for periodic modulation of Hα in our data. Clearly, a more sophisticated analy-
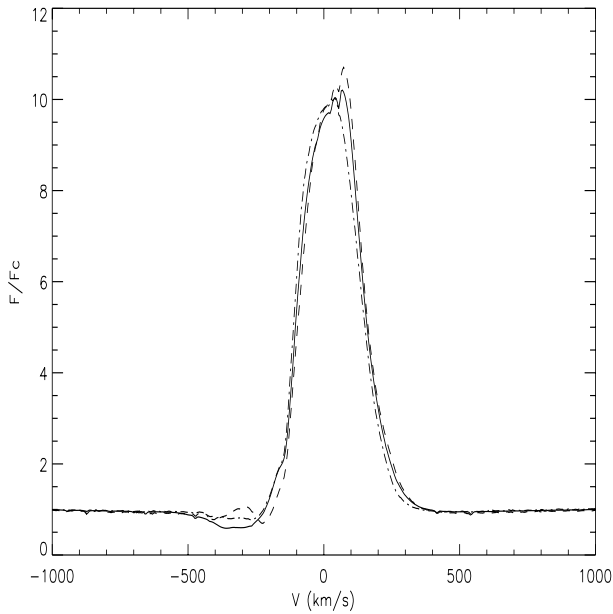
Fig. 19. Some of the Hα profiles. *Full line:* mean profile, averaged over the whole series; *Dashed line:* Nov. 22, 1996, 14.50 UT; *Dashed-dotted line:* Nov. 25, 1996, 2.52 UT
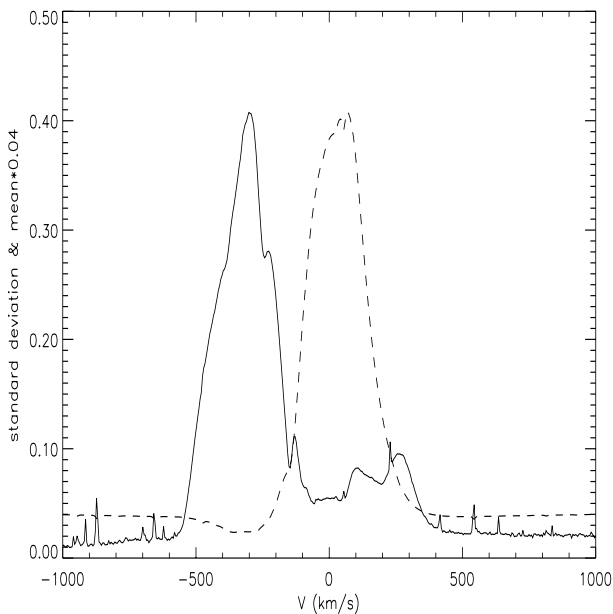
Fig. 20. The standard deviation across the Hα line profile, for the whole series (full line), divided at each velocity by the average line profile. The mean profile is given for reference (dashed line)
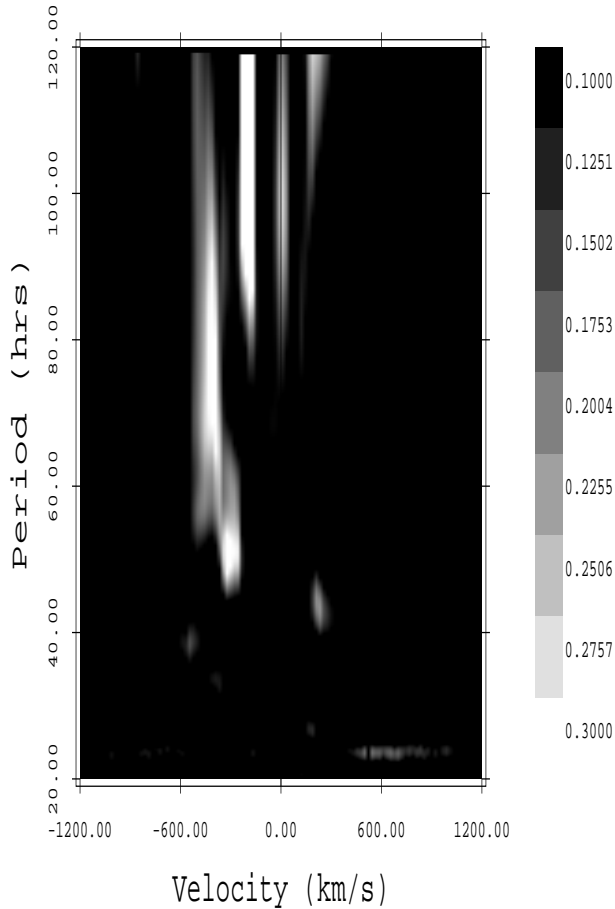

Fig. 21. Dynamic spectrum of the Hα line. The height of each spectrum does not correspond to the actual duration of the corresponding exposure, but has been increased for display purposes.

Finally, we note that a blue emission component, typical of type III P Cygni profiles, appears in spectra between t=80 and t=95 hrs, i.e., while both the blue edge velocity and the equivalent width of the blue component are smallest. This small emission is at a velocity which varies from $-330\,\mathrm{km\,s^{-1}}$ to $-310\,\mathrm{km\,s^{-1}}$ between t=80 and t=95 hrs. It does not re-appear later in the series, most likely because the absorption component always extends bluer than $-310\,\mathrm{km\,s^{-1}}$ after t=95 hrs.

5. Discussion

The behavior of AB Aur during the MUSICOS 96 campaign is far more complex than expected. It is beyond the scope of the present paper to give a complete picture of the atmospheric and envelope structures leading to such a complex variability. However, we make below a series of remarks based on the results presented above, that may play a decisive role in building a more complete model for this star.

The features that need to be accounted for in the modelling are summarized below:

sis, such as tomographic back-projection (Horne, 1991), would probably constitute a better approach to this particular set of data, and give us quantitative information about the peculiar behavior of the Hα absorption component, but this further analysis of our data is deferred to a subsequent paper.

It is interesting to notice that a strong widening of the Hα absorption component appears near t=65 hrs, at the same time as the same kind of phenomenon is seen in the He I D3 line.

Fig. 22. Two-dimensional period analysis of the Hα line. The periodogram is calculated according to Eq. (1).

1a. the photospheric lines have a very asymmetric profile, with a blue absorption component variable in position, modulated with a 34 hr period, and a red component in emission, at a more or less constant velocity, variable in amplitude, with a possible periodicity near 43 hrs.

1b. the shape of the photospheric lines is not exactly the same for lines of different ions.

2a. the He I D3 line exhibits two components, evolving differently.

2b. the blue emission component of the He I D3 line occurs at a velocity which is modulated with a 45 hr period; the modulation appears as a double wave for the first part of the campaign, then as a single wave.

2c. the red component, sometimes in emission and sometimes in absorption, does not vary significantly in velocity, but its intensity shows strong variations, with indications of a periodicity near 45 hrs.

2d. a dramatic event occurs about 65 hours after the start of the campaign, during which a strong wide absorption appears, centered at rest wavelength, both in the He I and the photospheric lines. This event coincides with a strong widening of the Hα blue absorption component. It also coincides with the change from

a double wave into a single wave modulation for the centroid velocity of the blue absorption component of the He I D3 line.

2e. the variations of the equivalent width of the the He I line are correlated with those of the photospheric lines (see Fig. 18); both sets of equivalent width variations are dominated by the behavior of the red half of the lines.

3a. the Hα line, presenting a P Cygni profile, is strongly variable, mostly in its blueshifted absorption component; on the other hand, the redshifted emission component is almost constant.

3b. there is no clear periodicity in the observed variations of Hα, although pseudo-periodic variations of its blue absorption component are suggested.

5.1. The photospheric lines

Strong perturbations of the photospheric layers are needed to explain the peculiar shape of the photospheric lines. In the following we discuss two of the three components appearing in the photospheric profile after subtracting a rotational profile (see Sect. 4.1): the blueshifted absorption component with a variable velocity modulated with a 34 hr period, and the low-velocity redshifted emission component with a mean velocity of $+25\,\mathrm{km\,s^{-1}}$. There is an additional high-velocity redshifted absorption component with a mean velocity of $+95\,\mathrm{km\,s^{-1}}$, but its existence is doubtful as argued in Sect. 4.1, and we shall not discuss it in detail here.

Since these two components behave differently, we first conclude that they originate from different parts of the stellar surface.

Let us first discuss the low-velocity redshifted component. The velocity of this component shows very little variation during the campaign. It is positive, but remains smaller than the rotation velocity. We conclude that this component probably originates from the polar region, since its velocity would be modulated by the star's rotation if it originated from lower latitudes, and that it is associated with a downflow occurring in this region. If the star is seen nearly edge-on, this implies large downward velocities. With the value of the inclination angle derived below, $i = 70°$, we need velocities of the order of $70\,\mathrm{km\,s^{-1}}$.

This component is variable in intensity. Whether or not these intensity variations are periodic could not be ascertained on the basis of the data presented here, but we do have some indication of a possible periodicity near 43 hrs.

We are finally led to conclude that one or several downflows onto the pole of AB Aur must be present, with velocities of the order of $70\,\mathrm{km\,s^{-1}}$, and which must be hotter than the underlying unperturbed photosphere, in order to produce an emission in the average photospheric line. In order to account for the variations in intensity of this component, we must assume that these downflows are variable in filling factor, density and/or temperature.

The velocity of the blue component behaves differently, with a periodic modulation between -40 and $-100\,\mathrm{km\,s^{-1}}$, with a 34 hr period. We may reasonably assume that this corresponds to the rotation period of the star's photosphere. Note that this period is very close to that observed in the Ca II K line by Catala

et al. (1986b), 32 hrs, also interpreted as the rotation period of the star. More recently, Gahm et al. (1993) have also reported some indication for a 35 hr period in photometric data of AB Aur, although with a low confidence level. Thus the variations of the blue component may be due to a peculiar structure of limited area at the photospheric level or at the base of the wind.

If the rotation period of the star is indeed 34 hrs, and if its projected rotation velocity is $85\,\mathrm{km\,s^{-1}}$, as we have adopted earlier, then we determine an inclination angle i of the order of $70°$, assuming a radius of $2.5\,R_\odot$, adequate for AB Aur (van den Ancker et al. 1997). However, this value is accompanied by a large error bar, considering the uncertainties on the projected rotation velocity, the modulation period and the stellar radius. We find that any inclination between $50°$ and $90°$ would be compatible with our data.

Important velocity fields must be present in the line formation region to account for our observations. Structures with no velocity fields (such as temperature or abundance inhomogeneities for instance) would produce perturbations crossing the line profile from blue to red, and extending as far to the red as to the blue. This is not what we observe here.

Similarly, horizontal velocity fields, such as e.g. meridional flows, cannot account for the observed blue component variations. Indeed, with the high inclination angle of the star's rotation axis implied by our data, such horizontal flows, if located at high latitude in the visible hemisphere or near the equator, will produce perturbations reaching almost as far to the red wing as they do to the blue wing, which is not observed; if located in the partly invisible hemisphere, such flows are seen only for a small fraction of the time, implying a very complex flow structure to account for the fact that the blue absorption component is seen in all of our spectra.

Conversely, we find that the observed blue component variations are compatible with radial flows in the photosphere. These radial flow structures must occur at high latitude, otherwise they would again produce perturbations extending significantly to the red for a significant amount of time. We have calculated that, for an inclination angle of the star's rotation axis of $70°$ as derived earlier, outward velocity fields of the order of $150\,\mathrm{km\,s^{-1}}$ at a latitude of $80°$ are necessary to explain the peculiar variability observed for the blue component.

Our observations can therefore be tentatively explained by:

(i) one or several expanding region(s) with velocities reaching up to $150\,\mathrm{km\,s^{-1}}$ in layers deep enough to contribute significantly to the formation of photospheric lines; these regions must be located at high latitude.
(ii) downflows onto the pole, with velocities of the order of $70\,\mathrm{km\,s^{-1}}$.

In the outflowing region, we may expect drastic changes in the density compared to the unperturbed stellar photosphere. Such density inhomogeneities will strongly affect the line formation, which may explain the large differences in the profiles of the photospheric lines of various species. As far as the downflow is concerned, we expect large temperature enhancements where the material hits the stellar pole, which again will affect strongly the formation of the lines. This latter effect may explain why the low-velocity redshifted component is seen in emission against the unperturbed photospheric line.

The possible 43 hr period seen in the intensity variations of the low-velocity redshifted component, if real, remains unexplained in the framework of this interpretation, although we may argue that it is somehow linked to the wind modulation which we describe in the next sections. However, as argued earlier, this apparent period may be simply due to the coincidental succession of two strong absorption events, at t=65 hrs and t=150 hrs.

5.2. The He I D3 line

This line is normally very weak in the spectrum of an A0V star like AB Aur. Its presence as a strong line, whether in absorption or in emission, indicates the existence of heated layers above the photosphere.

As for the photospheric lines, the He I line shows two components behaving quite differently. Since the red component does not vary significantly in velocity ($V \approx 100\,\mathrm{km\,s^{-1}}$), we conclude that it may also correspond to material falling inward onto the stellar pole. We note in this respect that the equivalent width of the He I line is well correlated with that of photospheric lines, the equivalent width variations being dominated by the behavior of the red half of the lines. We therefore conclude that the red components of the He I and photospheric lines originate from the same phenomenon, probably an accretion to the pole affecting both the upper layers where it creates the red component of the He I line and the photospheric layers where it creates the low-velocity red component of the photospheric lines. For an inclination angle of $70°$, we derive a velocity of the order of $300\,\mathrm{km\,s^{-1}}$ for the part of this downflow producing the He I red component.

This accretion must be variable to account for our observations. In particular, a strong modification of its characteristics must have occured near $t = 65$ hrs, to give rise to the dramatic event that we have already described earlier. The exact nature of this modification is not known for the moment.

The blue component of the He I line seems clearly modulated with a 45 hr period. It is also very tempting to interpret this periodicity as due to the stellar rotation. In the framework of this interpretation, the puzzle is to understand the period difference between the photospheric (34 hrs) and He I (45 hrs) line modulations. This result is reminiscent of the behavior of the Ca II K and Mg II h&k lines reported by Praderie et al. (1986) and Catala et al. (1986b), with periods of 32 hrs (Ca II K) and 45 hrs (Mg II h&k). An interpretation of these previous results was given by these authors in terms of a wind structure of fast and slow streams controlled by a surface magnetic field. According to this model, the Ca II K line is modulated by this structure, which rotates with the rotation rate of the star. Further away in the wind, the structure is destroyed, and the lines originating from the outer regions of the wind, like the Mg II lines, are modulated by the rotation of the envelope at that distance.

This model was acceptable because the Mg II lines are formed at great distances from the stellar surface (up to 50 R_*, see Catala et al. 1984), where indeed the stream structures are likely to have merged due to shocks at the interface between fast and slow streams. With the present set of data, we show that the He I line too is modulated with a longer period than the photosphere. The similarity between this period and that of the Mg II lines is striking. However, unlike the Mg II lines, this line cannot easily be formed at such great distances from the star, since it originates from very excited levels. The model presented in the past therefore cannot apply here. Moreover, since the period determined for the He I line is so close to that exhibited by the Mg II lines in the past, we may even argue that these new data contradict the previous model.

We are led to conclude that:
(i) either the wind is indeed structured into fast and slow streams rotating with the star, but in this case the different periods found in the data correspond to the rotation at different latitudes on the star; we shall call this "the equatorial wind" model; or
(ii) the wind does not originate from the stellar surface, but e.g. from a circumstellar disk, and the different periods exhibited by the different lines correspond to the rotation of the disk at different distances from the star; this model will be called "the disk wind" model.

We shall now examine these 2 different models in the light of the data presented in this paper. In both models, the photospheric lines are modulated by the rotation of a stream structure located at high latitude, and by a downflow of matter onto the stellar pole. The same downflow is also responsible for the red component of the He I D3 line.

5.3. The equatorial wind model

Clues for the existence of an equatorial wind in AB Aur and other Herbig stars were presented by Pogodin (1992). The best evidence is the repeated change from a P Cygni to a single emission profile at Hα, which is interpreted as a change in the latitude span of an equatorial wind: when the wind has a large opening angle, and extends to colatitudes below the inclination angle, the line of sight intercepts the expanding regions, and a P Cygni profile is formed. When this is not the case, the absorption component disappears, and Hα is left with a single emission.

If we adopt this idea, then we must consider that all wind lines are formed in a flow that originates from the equatorial regions of the star. Since we have many independent proofs of the presence of a strong stellar wind in AB Aur, through the various P Cygni profiles exhibited by some of its spectral lines, it is natural to assume that the blue component of the He I D3 line is formed in the wind, although pure accretion may also be capable of producing profiles like those of this line, as demonstrated by Hartmann et al. (1994) and Muzerolle et al. (1998). Bouret & Catala (1999) have recently produced a quantitative model in which this component is indeed formed in the inner region of the stellar wind. The Hα line is also obviously formed in the wind. Now this radial flow may be structured in fast and slow streams, which creates in the line profiles a modulation with the rotation

period of the star's equatorial regions. This phenomenon would be at the origin of the modulation seen in the blue component of the He I D3 line. This component is likely formed near the base of the wind, where the density is high enough to form this high excitation line (Bouret & Catala, 1999). Much further out in the wind, where the Hα absorption is produced, the streams may have merged, and the line may vary due to the rotation of these remote regions. In that case, no clear periodicity remains, since the Hα line is formed in an extended region with a broad range of rotation periods. The resulting variations may thus exhibit a complex behavior, as observed, with several inhomogeneities affecting the line formation at various distances from the star and creating line profile disturbances with different time scales.

The fact that the absorption component of Hα varies much more than its emission component (relatively) is easy to understand in the framework of this model: the absorption component indeed is formed in the regions of the wind that are projected on the stellar disk from the observer's point of view, which corresponds to a small volume. Any variation of the physical characteristics of this small volume will translate into a variation of the absorption component. On the other hand, the emission component is formed over the whole wind, which encompasses a very large volume. Therefore, the wind inhomogeneities are averaged out in this component.

The details of the He I line variations also suggest that the stream structure in the wind includes twice as many streams at the beginning of the campaign than at the end of the campaign, the change occurring near t=65 hrs.

If this interpretation is correct, then it indicates that the equatorial regions rotate more slowly than the high latitude regions, by as much as 20%. This is not totally surprising since the stellar wind is exerting a braking torque at the stellar surface, more efficiently at the equator than at the pole. Depending whether the resulting horizonthal shear is capable or not of quickly redistributing the angular momentum at the stellar surface, a strong latitudinal differential rotation will exist or not, with the pole rotating faster than the equator. This point deserves further modelling.

Such a high level of differential rotation must lead to a strong shear of the magnetic field lines, which must be entirely wound up in a time frame of approximately 150 hrs. If the photospheric structure responsible for the observed modulation is controlled by a magnetic field, we therefore expect this structure to evolve significantly on that time frame. This may actually be supported by the obvious change in the variability pattern of the photospheric line blue component at about t=160 hrs (see Fig. 7). The same argument may be applied to the He I line, formed in the wind, and also presumably modulated by the rotation of azimuthal structures in the wind, and may provide a qualitative explanation for the high level of "intrinsic" variation on top of a simple periodic modulation stressed by Böhm et al. (1996), as well as for the abrupt change in the modulation pattern exhibited by this line near t=65 hrs (see Fig. 14).

Finally, we have checked that such a differential rotation would not affect significantly the shape of the photospheric profile.

5.4. The disk wind model

Alternatively, we may assume that the wind is originating from a circumstellar disk, rather than from the stellar surface. A model of this kind has been recently proposed for massive young stars (Drew et a. 1998), in which an accretion disk is reprocessing the stellar luminosity, and the radiation pressure produced by this reprocessed flux is sufficient to lift up disk matter which is subjected only to the reduced gravitation from the disk. Although AB Aur is probably not luminous enough for this model to be directly applicable, it may be argued that rotation and magnetohydrodynamical effects can be added to radiation pressure for driving a disk wind in this star.

Accretion disk models have been proposed for Herbig Ae/Be stars in order to reproduce the observed IR excesses (Hillenbrand et al. 1992; Lada & Adams 1992). The mass accretion rates required by these models to be consistent with the observed IR energy distributions are very high, typically in the range 10^{-6}–10^{-5} $M_\odot$ yr^{-1}. This poses serious problems, and is in particular contradicted by the absence of optical veiling for the Herbig Ae/Be stars (Böhm & Catala 1993; Ghandour et al. 1994). On the other hand, the present photospheric data, showing a very distorted profile compared to a classical rotationally broadened profile, may hide a significant optical veiling. We must therefore consider this issue as still open.

The existence of optically thick accretion disks around most Herbig Ae/Be stars is also seriously questioned by the absence of asymmetry for the [O I] forbidden lines (Böhm & Catala 1994). Optically thick disks would indeed mask the receding parts of the stellar winds in which these lines are formed, which would result in a global blueshift of the line. Even though Corcoran & Ray (1997) have recently published a list of Herbig stars showing [O I] asymmetries, it remains true that many Herbig stars, including AB Aur, do not show any such asymmetries. On the other hand, Hirth et al. (1994) have suggested that the [O I] lines in Herbig Ae/Be stars may originate from a thin layer at the surface of an accretion disk, and therefore may not show any asymmetry even in the presence of disks. In this case, the emitting region must be very extended to account for the observed fluxes in the forbidden lines, and this prediction was recently contradicted by Böhm & Hirth (1997) on the basis of longslit spectra.

Recently, high angular resolution millimeter observations of Herbig Ae stars have revealed the presence of elongated structures around some of them, including AB Aur, on scales of several hundred AU (Mannings & Sargent, 1997). Such structures can be the signature of extended circumstellar disks around these stars. In particular, the evidence for keplerian rotation of molecular material in the elongated structure around AB Aur and HD 163296 makes a compelling case for circumstellar disks. However, these observations trace the stellar environment at several hundred AU from the star, and do not tell us much about the structure of the circumstellar material in the regions forming the lines we are studying here, which lie typically within 0.1 AU from the star.

All these results show that a high level of ambiguity still remains concerning the existence of thick accretion disks in the immediate environment of Herbig stars, and in particular around AB Aur. We also note that no observation precludes the existence of an optically thin disk.

The model we are discussing here therefore includes a rotating accretion disk around AB Aur, and a wind originating from this disk.

In the framework of this model, we do not need to invoke surface differential rotation to account for the different modulation periods derived from our data. The modulation of the photospheric lines is still due to the rotation of the inhomogeneous photosphere, with a period of 34 hrs. The periodic modulation of the lines formed in the wind is now due to the presence of inhomogeneities in the disk, producing local changes in the wind characteristics near its base (changes in velocity, density, and/or temperature). The spectroscopic signatures of these local wind changes are then modulated in velocity by the rotation of the disk structures to which they are anchored. We therefore expect to see a periodic modulation of the centroid velocity of the line components due to these inhomogeneities, with a period equal to the rotation period at the distance of formation of the line, $P_{\rm rot} = 2\pi r/V_{\rm rot}$, and with a total amplitude given by $a = 2V_{\rm rot}\sin i$, where $V_{\rm rot}$ is the rotation velocity at a distance r from the star center, and i the angle between the line of sight and the normal to the disk plane.

For the blue component of the He I line, we find a period of 45.1 hrs, and a total modulation amplitude of about 200 km s^{-1}. We have estimated i to about 70°, consistent with the value of 78° derived by Mannings & Sargent (1997) for the inclination of the circumstellar disk of AB Aur. These results would therefore imply that this component would be formed in the parts of the wind originating from the disk at about 1.6 R_*, which may perhaps correspond to the inner boundary of the accretion disk.

The disk rotation implied by our data (rotation period of 45.1 hrs at 1.6 R_*) is slower than keplerian, indicating that the accretion disk must lose a significant fraction of its angular momentum in the vicinity of the star, by a yet unknown mechanism. This conclusion is surprisingly opposite to the situation prevailing in the case of the classical T Tauri stars, where the angular momentum tends to be transferred from the disk to the star instead (Bouvier et al. 1993).

As in the case of the equatorial wind model, the Hα line is formed further out in the wind, and in regions which are more extended than those forming the He I line. The fact that the absorption component of Hα varies more than its emission component is easily understood, for the reason detailed in the previous section. We may also expect the observed complex behavior for the Hα line variations because the inhomogeneities responsible for them are distributed over regions of the disk with different rotation periods.

5.5. Downflows onto the stellar pole

In both types of models, we need to invoke downflows onto the pole of the star to account for the red components of the photo-

spheric and He I lines. These downflows need to have velocities of $300\,\mathrm{km\,s^{-1}}$ where they produce the He I red component, and of $70\,\mathrm{km\,s^{-1}}$ in the region of formation of the photospheric red component. Since the region of formation of the He I red component is probably located above that of the photospheric red component, we conclude that the downflows must be strongly decelerated as they approach the star's surface, possibly in a shock.

The intensity of the red components of the photospheric and He I lines seems to be modulated with a period near 45 hrs, suggesting that the characteristics of the polar downflows (accretion rate, temperature, geometry) may be modulated with this period. However, as detailed at the end of Sect. 4.3, this conclusion is not very reliable, so that we do not propose below a detailed interpretation of this phenomenon.

The origin of the material falling inward onto the stellar pole is not clear. It may be linked to the expanding regions at high latitude that we evidenced from the blue photospheric component, the stellar photospheric material first rising from a localized high latitude region, then falling back down on the pole, presumably being channelled in a magnetic canopy.

The material falling down on the stellar pole may also originate from the equatorial wind, channelled by a magnetic field. On the other hand, in the disk wind interpretation, the matter falling on the stellar pole may also originate from the disk itself in a magnetic accretion column.

Whatever the origin of these downflows, they must give rise to shocks near the stellar pole, where they will dissipate large amounts of kinetic energy. Rough estimates of the densities required to explain the red emission component of the He I line indicate mass accretion rates of the order of at least a few 10^{-9} $\mathrm{M_\odot\,yr^{-1}}$ (Bouret & Catala, 1999). The red component of the He I line indicates that these downflows have a typical velocity near $300\,\mathrm{km\,s^{-1}}$ in the regions forming the He I D3 line, and therefore carry a flux of kinetic energy of typically $E_{\mathrm{kin}} = 1/2\,\dot{M}v^2 =$ a few $10^{31}\,\mathrm{erg\,s^{-1}}$. The dissipation of this kinetic energy may provide an adequate explanation to the emission seen in the photospheric lines, and also partly explain the presence of superionized species like N V observed in HST/GHRS spectra (Bouret et al. 1997).

6. Conclusion

The main results of the MUSICOS 96 campaign on AB Aur are as follows:

- the photospheric lines exhibit a blue component in absorption with a velocity modulated with a 34 hr period, which we interpret as the rotation period of the stellar surface.
- the He I D3 line has a blueshifted emission component, whose velocity is modulated with a period near 45 hr. This modulation may be due to stream structures in an equatorial wind, the stellar equator rotating more slowly than higher latitude regions. Alternatively, this line may be formed in a wind from a rotating disk, at a distance of about $1.6\,\mathrm{R_*}$. In this case, we find that the disk rotation must be significantly slower than keplerian.

- both sets of lines have a red component, which is variable, with some indication of periodicity near 45 hrs. This component may be formed in downflows onto the stellar pole, originating either from the equatorial wind, or from the accretion disk in accreting columns.

The two alternatives presented in this paper to explain the observed variability have in common the presence of a wind, originating either from the equatorial regions of the star, or from a circumstellar inhomogeneous rotating disk. Also common to both models is the need for a highly structured photosphere involving significant radial velocity fields, as well as the presence of downflows onto the stellar pole.

In the equatorial wind model, we need to invoke surface differential rotation of the order of 25%, with the pole rotating faster than the equator, to explain the period difference between the modulation of the photospheric lines and that of the He I and other wind lines. This type of differential rotation is naturally expected in Herbig stars, which suffer a vigorous rotational braking because of their wind, preferentially at the equator. The wind azimuthal structuration is certainly produced by a surface magnetic field, yet undetected in AB Aur, but recently measured in another Herbig Ae star, HD 104237 (Donati et al. 1997).

In the disk wind model, the accretion disk needs to lose its angular momentum near the star surface, which is to be expected because of the unavoidable interaction between the star and the disk. The exact nature of this interaction is still unexplored, but it may provide an explanation for the large radiative losses observed in the heated regions above the photosphere. However, the observed symmetric and unshifted forbidden O I lines in AB Aur and other Herbig stars seem difficult to reconcile with the idea of an accretion disk capable of driving a wind at a mass loss rate of 10^{-8} $\mathrm{M_\odot\,yr^{-1}}$, and therefore necessarily optically thick. Such an accretion disk, by masking the receding part of the wind, would lead to blueshifted components in these forbidden lines, which are not observed.

Clearly, a lot of work remains to be done, both theoretically and observationally, to further study these two models, that we have just outlined in this paper.

References

van den Ancker M.E., Thé P.S., Tjin A Djie H.R.E., et al., 1997, A&A 324, L33
Babel J., Montmerle T., 1997, A&A 323, 121
Baranne A., Queloz D., Mayor M., et al., 1995, A&AS 119, 373
Baudrand J., Böhm T., 1992, A&A 259, 711

Beskrovnaya N.G., Pogodin M.A., Tarasov A.E., Scherbakov A.G., 1991, PAZh 17, 825

Beskrovnaya N.G., Pogodin M.A., Najdenov I.D., Romanyuk I.I., 1995, A&A 298, 585

Böhm T., Catala C., 1993, A&AS 101, 629

Böhm T., Catala C., 1994, A&A 290, 167

Böhm T., Catala C., Carter B., et al., 1996, A&AS 120, 431

Böhm T., Hirth G., 1997, A&A 324, 177

Bouret J.C., Catala C., Simon T., 1997, A&A 328, 606

Bouret J.C., Catala C., 1999, A&A, submitted

Bouvier J., Cabrit S., Fernández M., Martín E.L., Matthews J.M., 1993, A&A 272, 176

Catala C., Kunasz P.B., Praderie F., 1984, A&A 134, 402

Catala C., Czarny J., Felenbok P., Praderie F., 1986a, A&A 154, 103

Catala C., Felenbok P., Czarny J., Talavera A., Boesgaard A.M., 1986b, ApJ 308, 791

Catala C., Kunasz P.B., 1987, A&A 174, 158

Catala C., Böhm T., Donati J.-F., Semel M., 1993, A&A 278, 187

Catala C., Böhm T., Donati J.-F., et al., 1997, A&A 319, 176

Corcoran, M., Ray T.P., 1997, A&A 321, 189

Donati J.F., Semel M., Carter B.D., Rees D.E., Cameron A.C., 1997, MNRAS 291, 658

Donati J.F., Catala C., Wade G.A., Delaigue G., Rabou P., 1998, A&AS, in press

Drew J.E., Proga D., Stone J.M., 1998, MNRAS 296, L6

Finkenzeller U., 1983, A&A 124, 157

Finkenzeller U., Jankovics I., 1984, A&AS 57, 285

Gahm G.F., Gullbring E., Fischerstrom C., Lindroos K.P., Loden K., 1993, A&AS 100, 371

Ghandour L., Strom S., Edwards S., Hillenbrand L., 1994, In: The First Conference on the Nature and Evolutionary Status of Herbig Ae/Be Stars. ASP Conf. Ser. Vol. 62, 223

Hartmann L., Hewett R., Calvet N., 1994, ApJ 426, 669

Hillenbrand L.A., Strom S.E., Vrba F.J., Keene J., 1992, ApJ 397, 613

Hirth G.A., Mundt R., Solf J., 1994, A&A 285, 929

Horne K., 1986, PASP 98, 609

Horne K., 1991, In: Shafter A. (ed.) Proc. 12th North American Workshop on cataclysmic variables and XRBs

Kurucz R.L., 1979, ApJS 40, 1

Lada C.J., Adams F.C., 1992, ApJ 393, 278

Lignières F., Catala C., Mangeney A.C., 1996, A&A 314, 465

Mannings V., Sargent A.I., 1997, ApJ 490, 792

Marsh T.R., 1989, PASP 101, 1032

Muzerolle J., Calvet N., Hartmann L., 1998, ApJ 492, 743

Pogodin M.A., 1992, SvAL 18, 437

Praderie F., Simon T., Catala C., Boesgaard A.M., 1986, ApJ 303, 311

Scargle J.D., 1982, ApJ 263, 835

Vigneron C., Mangeney A., Catala C., Schatzman E., 1990, Solar Phys. 128, 287

Zinnecker H., Preibisch T., 1994, A&A 292, 152